Periodic Properties of Force Constants of Small Transition-Metal and Lanthanide Clusters

John R. Lombardi* and Benjamin Davis

Department of Chemistry and Center for Analysis of Structures and Interfaces (CASI), The City College of New York, Convent Ave. at 138th Street, New York, New York 10031

Received October 3, 2001

Contents

* To whom correspondence should be addressed. E-mail: lombardi@sci.ccny.cuny.edu.

I. Introduction

Understanding the electronic, physical, and chemical properties of metal clusters, for use in potential applications, is an issue attracting wide attention by large numbers of investigators working in diverse areas of research. This is especially evident from the proliferation of specialized symposia[1−6] and review articles,[7−10] where contributions have ranged from nuclear and solid-state physics through materials science and chemical synthesis. Interest in cluster science stems from the extensive knowledge we have about the physical properties of both atoms and metallic crystals. The relationship between atomic and metallic properties can be probed by following the attributes of clusters through a succession of various sizes. One approach would be to start with bulk materials and examine successively smaller particles. Another approach is to examine characteristics of successively larger clusters starting with dimers. It is this latter approach that we follow in the present work.

10.1021/cr010425j CCC: $39.75
Published on Web 04/27/2002

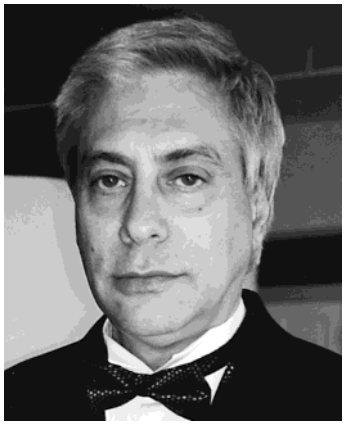

John R. Lombardi received his A.B. degree from Cornell University in 1963 and Ph.D. degree from Harvard University in 1967. He was Assistant Professor at the University of Illinois from 1967 to 1972, from which he was fired for his opposition to the war in Vietnam. After a year in Leiden, The Netherlands, and two years as a Visiting Professor at the Massachusetts Institute of Technology, he moved to the City College of the City University of New York, where he is currently Professor of Chemistry. His research interests have included high-resolution optical spectroscopy, Stark effects, Raman spectroscopy, and quantum theory of momentum space.

Benjamin L. Davis received a B.S. degree in Chemistry from Columbus State University in 1997 and his M.Phil. and Ph.D. degrees in Analytical Chemistry from the Graduate School of the City University of New York in 2001, where he studied photochemical hole-burning spectroscopy of porphryins and resonance Raman spectroscopy of mass-selected transition-metal clusters. He is currently a National Research Council Associate engaging in postdoctoral studies at the Naval Research Laboratory in Washington, D.C., where he is studying the light-harvesting characteristics of macromolecular dendrimers via static and time-resolved spectroscopy.

There are two dimensions to our considerations. One is the study of properties of a single metal with increasing cluster size. We wish to examine structural properties, such as bond strengths, geometries, and stabilities, with a view to determine the degree to which these properties can be used to understand and predict those of still larger clusters. The other dimension involves comparison of properties of individual metals across the periodic table in an attempt to extract the effect of the atomic origin of bonding electrons on cluster and bulk electronic properties.

In transition metals and lanthanides, s and d electrons dominate chemical bonding. Our interests lie in the extent of d-orbital contributions to possible multiple bonds. It is found that a wide variety of bond strengths are observed in transition-metal clusters, ranging from quite weak van der Waals bonding to some of the strongest chemical bonds (with bond orders as large as 5−6). It is clear that the availability of increasing numbers of d electrons, when traversing the periodic table, has a strong influence on the chemical bond strength. Periodic comparisons of bonding should provide insights as to the way in which s and d electrons interact to hold metal clusters together. Extension of these ideas to larger clusters, as well as correlations with bulk properties, is expected to provide a clearer picture of the nature of metal bonding.

Until recently it has been difficult to carry out such a program due to the unavailability of reliable experimental information as to the nature of bond strengths. However, advances in spectroscopic methods, especially application of several techniques of mass selection, have altered that picture. Mass selection removes any ambiguity as to the nature of the species under investigation. Various high-resolution spectroscopic tools have been invoked in order to enable the extraction of accurate and reliable structural parameters for a large portion of dimers and trimers as well as numerous larger clusters in the periodic table. With these methods we are currently in a position to examine the resulting trends.

It is the purpose of this article to review existing experimental data with a goal of understanding periodic trends in metal bonding and to gain insight on the degree to which properties of small clusters can be examined for understanding comparable properties in larger clusters. We owe a great debt to an earlier review by Morse,[8] which provides valuable data for an entire range of metal clusters. It is not our intention to present a similar review, which would be a monumental task, considering the enormous number of investigations that have been carried out since the late 1980s. Instead, we intend to focus almost entirely on experimental properties of homonuclear clusters with an emphasis on force constants. Data on the restoring force for small metal clusters have now been obtained for almost all transition-metal dimers as well as many trimers and several higher clusters. We will examine the degree to which these properties correlate with other measures of bonding, such as dissociation energies and equilibrium internuclear distances, and also properties obtained from ESR experimental methods, where useful. Also under scrutiny is the degree to which dimer force constants can be used as predictors of bonding strengths and other bulk properties in larger clusters.

Despite our emphasis on experimental properties, we should point out that enormous strides have been attained in various theoretical approaches, most notably in multiconfigurational self-consistent field (MCSCF) with multireference configuration interactions (MRSDCI) calculations[11] not to mention much recent exciting work in density functional theory (DFT).[12] However, since the theory is not yet at the stage for which sufficiently accurate force constants can routinely be obtained, we shall only refer to the theory when it can illuminate the experimental data. Theoretical calculations are especially valuable in predicting state orbital symmetries, which often cannot be directly obtained by experiment.

II. Experimental Techniques

Spectroscopic characterization of electronic energies of small transition-metal clusters yields structural information, physical properties, and insight into the nature of chemical bonding for these metallic molecules. In the past, typical spectroscopic experimentation on the ground state of metal clusters centered on the optical absorption and emission spectra of gas-phase clusters and additionally matrix isolation including Raman or IR studies. The main difficulty with early spectroscopic experiments was the cumbersome task of spectral interpretation due to the inability to isolate and identify specific metal cluster species. For such experiments a cluster sample was formed either by thermal sublimation or by flash photolysis and more recent laser vaporization of a bulk metal.[13−15] This process produced a gaseous cloud of metal clusters consisting of molecules with a wide range of cluster size as well as some impurities. At this point the sample was either probed in the gas phase or subsequently condensed into an inert matrix. Often, optical spectra displayed overlapping bands due to the presence of several different species. Even when separate spectroscopic transitions were observed, it was often difficult to unambiguously associate a transition with a particular cluster.

Within the past two decades experimental techniques concerning the spectroscopy of small metal clusters have evolved to take advantage of the high degree of specificity and detection sensitivity afforded by mass selection of these clusters. Mass selection is usually achieved by application of time-of-flight (TOF) mass spectroscopy or by utilizing one of several ion-filtering techniques such as quadrupole or Wien filters. The advent of mass-selected detection techniques such as resonant two-photon ionization (R2PI) of jet-cooled molecular metals,[16−20] negative-ion photoionization,[21−24] as well as various ion-filtering metal cluster beams make identifying the carrier of spectroscopic transitions unambiguous.[25−28] In an earlier review Bondybey, Smith, and Agreiter[29] discussed mass-selection techniques in conjunction with matrix isolation experiments.

Resonant two-photon ionization spectroscopy is a technique that allows for a high degree of accuracy when studying gas-phase metal clusters.[17] With most R2PI experiments, sample metal clusters are formed by laser vaporization of a bulk metal. Pulses of an inert gas, timed to coincide with the vaporization pulse, pass over the sample metal vapor. The inert gas quenches the plasma produced by laser vaporization and provides sufficient three-body collisions for metal cluster formation to occur.[16] The inert carrier gas, entrained with metal clusters, is then allowed to expand freely into an evacuated probing chamber, which further cools the clusters by way of supersonic expansion.[16] A wide distribution of rotationally and vibrationally cooled clusters is obtained by this process. In the probing chamber sample clusters are excited and ionized in a two-photon process. The ionized clusters are accelerated and detected by time-of-flight mass spectrometry. The magnitude of the ion current is greatly enhanced when the exciting laser wavelength is scanned through a resonance. The resulting spectrum provides very high resolution, while the mass-spectroscopic detection allows extremely high sensitivity. This technique provides accurate spectroscopic information on neutral excited-state lifetimes and adiabatic ionization potentials arising from a species of known mass.

Another mass selection/spectroscopic method used to isolate small metal clusters of specific cluster size is negative-ion photoelectron spectroscopy. Anions of metal clusters are prepared by a flowing afterglow ion source.[21] After the creation of sample anionic clusters, the negatively charged molecules are mass-selected, usually utilizing a Wien filter, which utilizes crossed electric and magnetic fields to focus species of a single chosen charge-to-mass ratio. Once separated, an ionizing source (such as a CW Ar^+ laser) supplies sufficient energy to cause photodetachment of electrons. This process forms neutral clusters and electrons of discrete kinetic energies.

Information on the neutral clusters is extracted by measuring the kinetic energies of photoejected electrons. The photoelectrons are detected using a hemispherical analyzer for energy analysis. This is coupled to a microchannel plate detector, which counts the number of photoelectrons at the transmitted kinetic energy. Because the hemispherical analyzer may be set to transmit electrons of any energy, this experimental method allows low-energy states to be probed. These may be difficult to access using other spectroscopic methods.[21] Resolution on the order of 10−20 cm^{-1} is obtainable for probed kinetic energies of photodetached electrons.

A related technique pioneered by Wang and coworkers[30] utilizes laser vaporization/magnetic-bottle time-of-flight mass spectroscopy to probe the photoelectron spectroscopy of series of clusters over a wide range of cluster size. For example, Fe_n^- clusters were examined up to $n = 34$. The examination of electron affinities, ionization potentials, and chemical reactivity are exploited to reveal the onset of bulk behavior.

R2PI and negative-ion photoelectron spectroscopy primarily study mass-selected small metal clusters in the gas phase. Another useful technique is to probe mass-selected metallic species in an inert matrix via resonance Raman spectroscopy. This may be accomplished by ion plasma sputtering of a bulk metal, followed by Wien filter mass selection of the cationic molecules, and subsequent matrix isolation of the species. As of now, there are three such facilities. One in Lausanne, Switzerland, constructed by W. Harbich,[31,32] another originally in Toronto, Canada, built by M. Moskovits[33], and ours here at CCNY. The ability to mass select metal clusters gives a resonance Raman spectrum devoid of interference from spectral bands and progressions due to unwanted clusters. Similar to R2PI and negative-ion photoelectron spectroscopy, acquired optical spectra from a metal cluster beam provides a clear and unambiguous assignment which can only be due to a single species.

A typical metal cluster beam is shown in Figure 1. An argon ion beam sputters a water-cooled metal target causing the formation of cluster cations. These cations are extracted from the metal sputtering

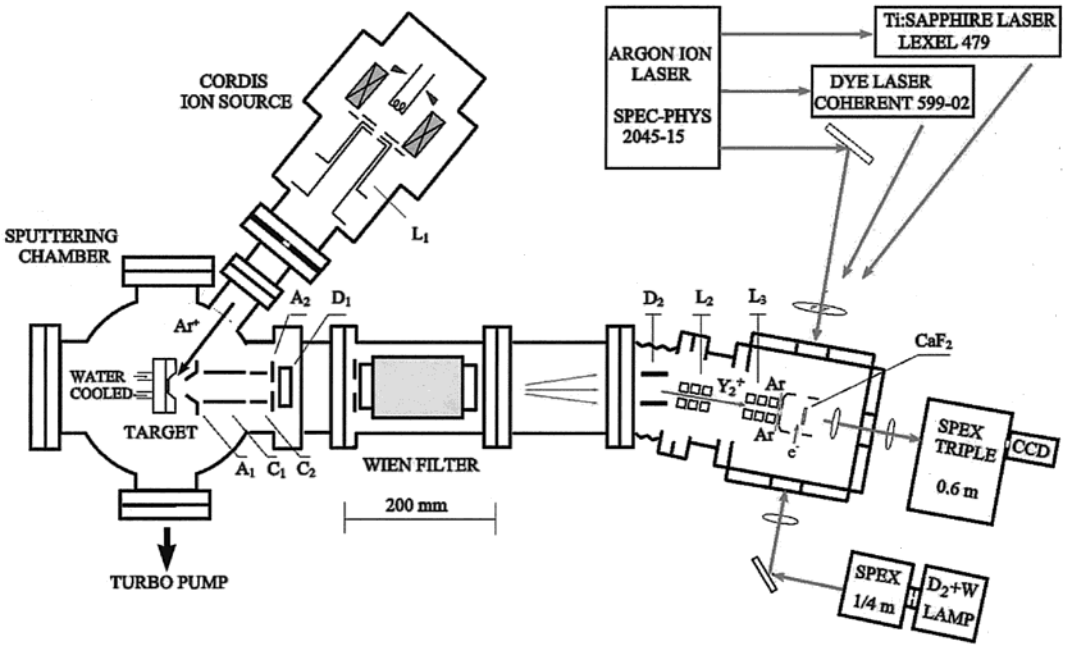

Figure 1. Schematic of a typical metal cluster deposition source. Metal cluster ions are sputtered from a metal target by accelerated argon ions produced in the Cordis ion source. They are directed by a series of Einzel lenses (A and C) to a Wien filter, which deflects all ions except those selected. The mass-selected ions are then slowed, neutralized by electrons from a tungsten filament, and co-deposited with argon on a cooled CaF_2 plate. The matrix-isolated sample may then be examined spectroscopically by various absorption, fluorescence, and Raman techniques.

chamber, and the focused metal cluster cations are mass selected via a Wien filter. Mass selection resolution ($M/\Delta M$) for such experiments is ~6−7, which is sufficient for separation of cluster cations ranging from dimers to tetramers from the metal atom and to ensure that oxides are not present. Mass-selected cluster cations are focused by two Einzel lenses into the deposition chamber and are co-deposited with argon gas and electrons, for neutralization, onto a CaF_2 substrate, usually maintained at ~16 K. This "soft landing" technique is designed to reduce fragmentation and enable ordered rare-gas matrices to be grown without disruption due to high kinetic energies of incoming ions. The degree of cluster fragmentation is estimated by comparing the intensities of atomic excitation features in a mass-selected cluster deposition with those obtained from depositions of the atom under similar conditions. Fragmentation ratios for these experiments are usually ≤15%. It is found that this value is strongly correlated with the dissociation energy of the parent species.

Matrix samples are probed in situ via absorption and resonance Raman spectroscopy. Absorption spectra for selected cluster samples are obtained via a "scattering depletion spectrum" (SDS). With SDS, a ratio between scattered light from the center of the substrate, where most of the sample has been deposited, and scattered light from the edge of the substrate is collected at a 90° angle relative to the incident light. Resonance Raman experiments are carried out using the visible lines of an argon ion laser and various dye laser lines as well as a Ti sapphire laser. Results from application of the above techniques have enabled the various researchers to obtain information on ground-state vibrations, anharmonicities, force constants, dissociation energies, and geometrical parameters of many dimers and trimers of transition metals and lanthanides as well as scattered results on larger clusters. In the next section we review the experimental parameters/results obtained, which have been collected and are displayed in several of the following tables.

III. Summary of Experimental Results

A. Group 3

1. Scandium

The ground state of scandium dimer (Sc_2) has been established to be $^5\Sigma_u^-$ by ESR[34] as well as density functional calculations.[35] This state derives from the interaction of one ground-state $4s^23d^1(^2D)$ atom with one excited-state $4s^13d^2$ (^4F, 1.43 eV)) atom. The $^5\Sigma_u^-$ state derives from a $\sigma_g^2\sigma_u^1\pi_u^2\sigma_g^1$ configuration in which the $\sigma_g^2\sigma_u^1$ portion correlates with the $4s^2 + 4s$ portion of the separated atom wave function while the remaining $\pi_u^2\sigma_g^1$ portion represents the 3d bonding between the two atoms. This implies considerable s−d hybridization in these systems. Using resonance Raman spectroscopy, Moskovits, DiLella, and Limm[36] found a ground-state vibrational frequency of $\omega_e = 239.9\ cm^{-1}$ and $\omega_e x_e = 0.93\ cm^{-1}$. Several values have been reported for the dissociation energy. Using third-law measurements, Gingerich[37] found $D_0 = 1.65(22)$ eV. Verhaegen et al.[38] reported a value of 1.12 eV. In a reanalysis of the latter value using a LeRoy−Bernstein analysis and updated molecular parameters, Haslett et al.[39] concluded that a lower limit of 0.79 eV was the best that could be obtained from the data. Given the ambiguities in interpretation of the lower value, we choose the value of 1.65 eV as more likely to be correct.

The ground state of scandium trimer (Sc_3) was shown by Knight et al.[40] using ESR measurements to be $^2A_1'$ (D_{3h}) symmetry. Walch and Bauschlicher[41] calculate a low-lying $^2E'$ state which is also recommended by Moskovits et al.[36] in a matrix isolation Raman study. Vibrational frequencies of $\omega_a = 248$ cm^{-1} (a_1') and $\omega_e = 150$ cm^{-1} (e') were obtained. At lower temperatures, this latter frequency is actually split into 145 and 151 cm^{-1} but coalesces as the temperature is raised, confirming the D_{3h} symmetry obtained from ESR.

2. Yttrium

In a mass-selected resonance Raman matrix isolation study of Y_2, Fang et al.[42] found $\omega_e = 184.4$ cm^{-1} and using Badger's rule suggest a value of $r_e = 2.65$ Å. The vibrational frequency is in substantial agreement with that (185 cm^{-1}) obtained by PFI-ZEKE spectroscopy,[43] which also provided evidence for a $^5\Sigma_u^-$ ground state. As in scandium, this state derives from the interaction of one ground-state $5s^24d^1(^2D)$ atom with one excited-state $5s^14d^2$ (^4F, 1.36 eV)) atom. Calculations by Dai and Balasubramanian[44] agree with the ground-state designation but suggest a nearby low-lying $^1\Sigma_g^+$ as an alternative. The dissociation energy of $D_e = 1.62(22)$ eV was obtained using mass-spectrometric means by Verhaegen, Smoes, and Drowart.[38]

An ESR study by Knight et al.[40] indicates a $^2B_2$ (C_{2v}) structure for the ground state of the trimer.

3. Lutetium and the Lanthanides

Seven of the lanthanide dimers, including La_2,[45] Ce_2,[27] Pr_2,[27] Nd_2,[27] Gd_2,[28] Tb_2,[46] and Lu_2,[47] have been examined using mass-selected matrix isolation resonance Raman spectroscopy. Even though lanthanides are extremely oxophilic, there is little evidence of oxides in the mass-selected cluster apparatus due to the ultrahigh vacuum obtained. Using a residual gas analyzer, the levels of oxygen and water impurities are found to be low, and furthermore, the Raman frequencies of the lanthanide oxides are well-known and not observed in the spectra. The observed vibrational frequencies are 236.0, 245.4, 244.9, 148.0, 138.7, 137.6, and 121.6 cm^{-1} respectively. The remaining dimers were not examined since they were more likely to be unstable either in a sputtering source or easily fragmented under typical deposition conditions due to the rather low value of their thermodynamic dissociation energies. Note that we use lutetium rather than lanthanum as the header in this position in the periodic table. We discuss the reasons for this below in the section on lanthanides.

B. Group 4

1. Titanium

In a study of jet-cooled titanium dimers (Ti_2), Doverstal, Karlsson, Lindgren, and co-workers[18,48] carried out a rotational analysis. They found a $^3\Delta_g$ ground state with an equilibrium internuclear distance of $r_0 = 1.9422(8)$ Å. They note that this assigned ground-state symmetry stems from a $4s\sigma_g^2\ 3d\sigma_g^1\ 3d\pi_u^4\ 3d\delta_g^1$ configuration, which implies an unusual orbital ordering. This has been explained by 4s−3d hybridization. Cooper, Clarke, and Hare[49] suggest dissociation of the dimer to two atoms with $3d^34s^1$ configuration. Cosse et al.,[50] in a laser-excited resonance Raman spectrum, find $\omega_e = 407.9$ cm^{-1}. Kant and Lin,[51] using effusion and mass-spectrometric techniques, found the dissociation energy to be $D_0 = 1.40$ eV.

2. Zirconium

In a resonant two-photon ionization spectrum of jet-cooled zirconium dimer (Zr_2), Doverstal, Karlsson, Lindgren, and Sassenberg[52] found a $^3\Delta_g$ ($\Omega = 1$) ground state from a $(5s\sigma_g)^2(4d\sigma_g)^1(4d\pi_u)^4(4d\delta_g)^1$ configuration dissociating to two atoms in the ^5F state. They also determined that $r_0 = 2.2407(21)$ Å. Mass-selected resonance Raman spectra in matrix isolation[53] resulted in $\omega_e = 305.7$ cm^{-1} and $\omega_e x_e = 0.5(7)$ cm^{-1}. Arrington et al.[54] found an abrupt dissociation threshold in the optical spectrum to obtain a value of $D_0 = 3.052(1)$ eV.

Haouri et al.[55] found $\omega_a = 258.0$ cm^{-1} and $\omega_e = 176.7$ cm^{-1} in mass-selected resonance Raman spectroscopy of the trimer of zirconium in matrix isolation. The results indicate an equilateral triangle (D_{3h}) geometry with a stretching force constant of 1.95 mdyne/Å and a stretch−stretch interaction constant of 0.05 mdyne/Å. This is in contrast to the apex angle of 71° and C_{2v} geometry suggested for a $^1A_1$ state by the calculations of Dai and Balasubramanian.[56]

3. Hafnium

Very little work has been carried out on Hf clusters. The resonance Raman spectrum of mass-selected hafnium dimers (Hf_2) in argon matrices was obtained by Hu et al.[57] Ground-state vibrational frequencies of $\omega_e = 176.2(26)$ cm^{-1} and $\omega_e x_e < 1$ cm^{-1} were obtained. Morse[8] recommended the value of 3.4(6) eV for the dissociation energy of the dimer, and we adopt that value here, although there no direct experimental evidence for this value and it must be regarded as suspect.

The spectrum of the trimer (Hf_3)[58] has also been obtained and analyzed. Several transitions were observed in the visible region of the absorption spectrum. They appear broad and featureless in the 605−620 nm region. The Raman spectrum is too complex to be attributed to a single ground state. Instead, the observed spectrum may be explained by five additional low-lying excited states, which are labeled A, B, C, D, and E at 319.0, 413.4, 609.6, 642.8 (weak), and 785.4 cm^{-1}, respectively. The ground-state X shows complex structure which may be interpreted as the result of a strong, linear Jahn−Teller effect. Evidence is obtained of a pseudorotational structure with states of vibronic angular momentum of $j = 1/2, 3/2, 5/2, 7/2$ and an a_1' normal frequency of 142.8 cm^{-1}. This indicates a fluxional ground state with either E′ or E″ symmetry in the D_{3h} limit. No such effects are apparent in the low-lying excited states, although a_1' modes of 143−152 cm^{-1} are observed and in some cases geometrical information may be obtained. The A state (319.0 cm^{-1}) is geometrically an equilateral triangle (D_{3h}).

The B state (413.4 cm^{-1}) shows an a_1' vibration, but without an observed nontotally symmetric mode, no geometrical information can be inferred. The C state (609.6 cm^{-1}) shows only a nontotally symmetric mode at 116.7 cm^{-1}, while the D state (642.8 cm^{-1}) and the E state (785.4 cm^{-1}) both appear to be D_{3h}. The excitation profiles appear as several distinct types, indicating that the optical bands may be further resolved in peaks at 606, 610, 615, and 619 nm.

In a recent theoretical article, Dai, Roszak, and Balasubramanian carried out CAS-MCSCF calculations followed by multireference configuration interactions (MRSDCI) on Hf_3 using up to 2.23 million configurations.[59] They suggest that the ground-state derives from a $^3E''$ (in D_{3h}) split by Jahn−Teller coupling into a $^3A_2$ ($\theta = 63.0°$) and a $^3B_1$ ($\theta = 67.7°$) state. They point out, correctly, that for such a heavy molecule, spin−orbit interactions should quench Jahn−Teller coupling. Their estimate for the Jahn−Teller stabilization energy is only 0.04 eV, while the spin−orbit interaction lowers the $^3A_2$ state by 0.65 eV. Their calculated vibration frequencies (166.1 and 102.5 cm^{-1}) are remarkably close to the experimental results.

C. Group 5

1. Vanadium

Several measurements of the ground-state vibrational frequency of divanadium (V_2) have been made, and they are in substantial agreement. In the gas phase, Langridge-Smith et al.[60] obtained a value of $\Delta G_{1/2} = 529.5(10)$ cm^{-1} while Cosse et al.[50] obtained $\omega_e = 537.5$ cm^{-1} and $\omega_e x_e = 4.2$ cm^{-1} in matrix isolation Raman spectra. With mass-selection techniques, the resonance Raman spectrum[26] yielded the values of $\omega_e = 536.9(11)$ cm^{-1} and $\omega_e x_e = 4.1(1)$ cm^{-1}. Density functional calculations[61] confirm the result of Langridge-Smith et al.[60] that the ground state is most likely a $^3\Sigma_g^-$ deriving from a $4s\sigma_g^2\ 3d\sigma_g^2\ 3d\pi_u^4\ 3d\delta_g^2$ configuration. Spain, Behm, and Morse[20] obtained $r_e = 1.77$ Å for the equilibrium internuclear distance and a dissociation energy of 2.75 eV, while Spain and Morse[62] indicate dissociation to two $3d^3$-$4s^2$ atoms. The s−d promotion energy is only 0.26 eV, so that the resulting diabatic dissociation energy $D_0^d = 3.27$ eV.

Little work exists on the trimer. Calaminici et al.[61] carried out density functional calculations and predict a $^2A'_1$ (D_{3h}) ground state with $r_e = 2.169$ Å and frequencies of 421 and 255 cm^{-1} and a low-lying $^4A_2$ (C_{2v}) (0.03 eV) excited state resulting from a Jahn−Teller distortion. However, in a fit to the PFI-ZEKE spectrum,[63] Yang, James, and Hackett provide evidence that the $^2A'_1$ is indeed the ground state.

2. Niobium

Resonance Raman matrix isolation spectra of niobium dimer (Nb_2) were originally studied by Moskovits and Limm,[64] who obtained $\omega_e = 421$ cm^{-1} and $\omega_e x_e = 1.4$ cm^{-1}. Using mass-selected techniques, Hu et al.[65] obtained substantially the same result $\omega_e = 420.5(5)$ cm^{-1} and $\omega_e x_e = 0.5(3)$ cm^{-1}. Both are in agreement with the rotationally resolved gas-phase laser vaporization study,[66] which found $\omega_e = 424.9$ cm^{-1}. They also showed the ground state to be a $^3\Sigma_g^-$ stemming from a $1\pi_u^4\ 1\sigma_g^2\ 2\sigma_g^2\ 1\delta_g^2$ configuration. A value for the equilibrium internuclear distance of $r_e = 2.07781$ Å was obtained. In a later study from the same laboratory[67] a dissociation energy of $D_0 = 5.48$ eV was reported. These results all indicate a rather strong chemical bond with a formal bond order of 5.

The mass-selected trimer resonance Raman spectrum was obtained by Wang et al.[68] D_{3h} equilateral triangle geometry was obtained with a likely $^2E'$ ground state. The vibrational constants were $\omega_a = 334.9(28)$ cm^{-1} and $\omega_e = 227.4(29)$ cm^{-1}, and a normal coordinate analysis indicates a stretching force constant of $k_e = 1.95$ mdyne/Å and a stretch−stretch interaction constant of 0.05 mdyne/Å. Leopold[69] observed a long progression in 220 cm^{-1} for Nb_3 using negative-ion photoelectron spectroscopy. This most likely corresponds to the degenerate bend ω_e.

3. Tantalum

Tantalum is the only metal for which force constant data from mass-selected Raman matrix isolation is available for the dimer, trimer, and tetramer. Heaven et al.[70] showed in a density functional calculation that the ground state of the dimer (Ta_2) is $^1\Sigma_g^+$. In a mass-selected resonance Raman matrix isolation experiment, Hu et al.[71] obtained $\omega_e = 300.2(12)$ cm^{-1} and $\omega_e x_e = 4.80(4)$ cm^{-1}. Only the symmetric stretch vibrational frequency could be observed in the trimer (Ta_3) with $\omega_a = 251.2$ cm^{-1}.[72] Heaven et al. recommend a $^2A''(C_s)$ ground state, although there is no experimental evidence to corroborate this and it is highly unlikely since such geometry has not been observed for any other transition-metal trimer. In the tetramer (Ta_4) it was shown[73] that the molecule is of tetrahedral (T_d) symmetry and, since a weak Jahn−Teller effect is observed, that the ground state is electronically E. (The T electronic state was excluded since the vibronically coupled vibration is of e symmetry and only the vibrations of the same symmetry can be coupled in the Jahn−Teller effect.) Three vibrational fundamentals are observed at $\omega_a = 270.2(1)$ cm^{-1}, $\omega_e = 130.6(2)$ cm^{-1}, and $\omega_t = 185.1(1)$ cm^{-1}. The Jahn−Teller coupling parameter is $\lambda = 0.017(2)$. The observed ratio of the totally symmetric stretch (a_1), the triply degenerate (t), and the doubly degenerate (e) vibration $\{\omega_a:\omega_t:\omega_e\}$ of $2:\sqrt{2}:1$ provide confirmation of the tetrahedral geometry in the central force approximation.[74]

D. Group 6

1. Chromium

There has been considerable work carried out on chromium dimer (Cr_2). The ground state is $^1\Sigma_g^+$. Bondybey and English[75] produced Cr_2 in a pulsed YAG laser vaporization source and obtained high-resolution rotational fluorescence excitation spectra. They determined a value of $r_e = 1.6788$ Å and a very accurate value of $\Delta G''_{1/2} = 452.34$ cm^{-1}. These results indicate a closed-shell $(3d\sigma_g)^2(3d\pi_u)^4(3d\delta_g)^4(4s\sigma_g)^2$ leading configuration (among others) with a formal bond order of 6. Using photoelectron spectroscopy, Casey

and Leopold[76] found over 30 ground-state vibrational levels indicating an extremely anharmonic potential and requiring anharmonic terms up to sixth order for an adequate fit. This was interpreted as due to a shelf-like potential stemming from a rate of dissociation of the relatively diffuse 4s-bonded electrons, which is distinct from the rate at which dissociation occurs in the more compact 3d electrons. The resulting *harmonic* frequency was found to be 480.6 cm^{-1}, giving a force constant of 3.53 mdyne/Å. This value is higher than that of any other first transition dimer except V_2. Two accurate values of the dissociation energy have been reported. One by Hilpert et al. is 1.443 eV,[77] while another by Simard et al.[78] is 1.53-(6) eV. These values are even lower than that of singly bonded Cu_2 (2.03 eV). This apparent disparity between a high force constant and a rather low dissociation energy in Cr_2 is clearly due to the considerable distortion of the potential function. This provides a clear indication of the ways in which force constants and dissociation energies are sensitive to different aspects of chemical bonding.

DiLella et al.[79−81] report a matrix isolation Raman spectrum of Cr_2 in which they obtain $\omega_e = 427.5$ cm^{-1} and $\omega_e x_e = 15.8$ cm^{-1}. However, in a recent mass-selected study,[82] it has been shown that these frequencies are instead characteristic of the trimer. The mass-selected experiment shows totally symmetric and degenerate bending modes of $\omega_a = 432.2$ cm^{-1} and $\omega_e = 302.0$ cm^{-1}. Their ratio is almost exactly $\sqrt{2}$, indicating D_{3h} symmetry for the trimer.

2. Molybdenum

The dimer of molybdenum has a $^1\Sigma_g^+$ ground state. In a high-resolution emission and absorption study of Mo_2 produced by flash photolysis, Efremov et al.[14] found the ground-state vibrational frequency $\omega_e = 477.1$ cm^{-1} and $\omega_e x_e = 1.51$ cm^{-1}. A rotational analysis showed $r_e = 1.929$ Å. In matrix isolation fluorescence spectra of Mo_2, Pellin et al.[83] found essentially the same value for ω_e. Simard et al.[84] found $D_0 = 4.476$ eV using photoionization spectroscopy. Recently a mass-selected resonance Raman spectrum[85] of Mo_2 has been obtained in matrix isolation. Surprisingly, three fundamentals were observed at 394.5, 446.0, and 473.3 cm^{-1}. At liquid helium temperatures, these cannot be due to thermal population of excited levels, so that at least two of these values must represent optical pumping into excited states. The last two match an excited state and the presumed ground-state frequency obtained by Efremov et al., while the first is both most intense and resonantly enhanced. In a recent Fourier transform study of laser-vaporized Mo_2 trapped in solid Ne, Kraus, Lorenz, and Bondybey[86] found a new IR transition to a $^3\Sigma_u^+$ state at 8032.2 cm^{-1} with $\omega_e = 393.7$ cm^{-1}. This is most likely the state from which the lowest Raman line was observed. Note that the higher frequency line leads to a force constant of 6.433 mdyne/Å. If correct, this represents a bond order of 5 or 6, making it one of the strongest bonds ever observed.

The trimer was also observed in the previously mentioned mass-selection studies,[85] and the resonance Raman spectra showed a totally symmetric stretch of $\omega_1(a_1) = 386.8$ cm^{-1}, the antisymmetric stretch $\omega_2(b_1) = 224.5$ cm^{-1}, and the bend at $\omega_3(a_1) = 236.2$ cm^{-1}. This indicates C_{2v} symmetry with an apex angle of 83.7°.

3. Tungsten

The only spectroscopic data on tungsten dimer (W_2) was obtained in a mass-selected matrix isolation study by Hu et al.[87] They obtained a value of $\omega_e = 336.8(7)$ cm^{-1} and $\omega_e x_e < 1$ cm^{-1} and suggest the most likely ground-state symmetry is $^1\Sigma_g^+$. Morse[8] suggests a dissociation energy of $D_e = 5(1)$ eV.

E. Group 7

1. Manganese

The ground state ($^1\Sigma_g^+$) of the manganese dimer (Mn_2) is a van der Waals molecule stabilized by antiferrromagnetic exchange interaction between the d^5 electrons on each atom.[88] The atomic configuration of Mn is $3d^54s^2$ with a very high promotion energy, and this especially stable configuration resists facile bonding. The result is a rather long internuclear distance of 3.4 Å[89], a low dissociation energy $D_0 = 0.1$ eV[90], and a very low vibrational frequency $\omega_e = 76.4$ cm^{-1} and $\omega_e x_e = 0.53$ cm^{-1}.[91] These are all characteristic of extremely weak chemical bonding. Although the observed frequencies were observed in matrix isolation, which in the case of very weak bonding can seriously distort the observed frequencies (compared with gas phase results), these are currently the best measurements available.

Manganese trimer was investigated using matrix isolation Raman spectroscopy by Bier, Haslett, Kirkwood, and Moskovits.[91] They found an equilateral triangle E′ or E″ (D_{3h}) ground state with dynamic Jahn−Teller coupling. The vibrational constants were $\omega_a - 2x_a = 196.8$ cm^{-1}, $\omega_e = 130.2$ cm^{-1}, and a Jahn−Teller coupling parameter of 2.95 cm^{-1}. They were able to reproduce these parameters with a bond stretch force constant of $k_e = 0.38$ mdyne/Å and a stretch−stretch interaction force constant of 0.02 mdyne/Å. Note that the trimer force constant is over four times that of the dimer, indicating a change in bonding between the dimer and trimer. It is clear that for the trimer, covalent bonding has replaced van der Waals interactions as the dominant mode.

2. Technetium

Due to its mild radioactivity and high cost, little work has been carried out on technetium. For the dimer, Brewer and Winn[92] suggest a D_0 of 2.93 eV while Miedema and Gingerich[93] report $D_0 = 3.43(10)$ eV. From these values it is clear that the bonding is considerably greater than that in Mn_2, resembling more that of Re_2. This is due to the fact that Tc has a low 5s−4d promotion energy (0.41 eV compared to 2.14 eV for Mn) and the 4d and 5s orbitals are more comparable in size, allowing d-orbital participation in bonding. This is confirmed by the fact that several strongly bound ligated species have been synthesized. For example,[94] the Tc−Tc bond distance in $Tc_2Cl_8^{3-}$ is only 2.117(2) Å.

3. Rhenium

Experimental work in matrix isolation on the rhenium dimer (Re_2) was carried out by Hu et al.[25] using mass-selected techniques. The absorption spectrum was unusually rich and sharp for a transition-metal cluster, enabling the measurement of vibrational constants for eight excited electronic states, and both resonance Raman and fluorescence spectra were observed to the ground state. The dirhenium absorption spectrum consists of seven band systems (A−G) extending from the near-infrared into the ultraviolet region. For the A system (a simple vibrational progression) $T_0 = 10\,817(1)$ cm^{-1}, $\omega_e = 317.1(5)$ cm^{-1}, and $\omega_e x_e = 1.0(1)$ cm^{-1}. The spectra indicate that dissociation of the ground state is to $5d^56s^2 + 5d^66s^1$ atomic configurations. A Franck−Condon analysis of the A system intensities predicts that this state has a smaller equilibrium internuclear distance than the ground state ($\Delta r_e = -0.073$ Å), in violation of Badger's rule. The B system starts at 13 250 cm^{-1} and consists of four overlapping (and possibly perturbed) subsystems, whose average vibrational spacing is 270(11) cm^{-1}. The C, D, E, and F systems (vibrational spacings in parentheses) are centered at 22 300 (210 cm^{-1}), 24 500 (195 cm^{-1}), 29 150 (175 cm^{-1}), and 32 900 cm^{-1} (160 cm^{-1}), respectively. Weak fluorescence spectra, obtained upon laser excitation into the A system, were characterized by vibrational progressions to the dimer ground (X) state and to a low-lying (X′) state for which $T_0 = 357.6(5)$ cm^{-1} and $\omega_e = 332.3(2)$ cm^{-1}. Raman and fluorescence progressions to the ground state were observed when the B system was excited. The ground state is most likely a 1_g ($^3\Delta_g$), and the values of $\omega_e = 337.9(49)$ cm^{-1} and $\omega_e x_e = 0.1(7)$ cm^{-1} were obtained. Photodetachment spectroscopy[95] showed $\omega_e = 340(20)$ cm^{-1}, in agreement with the Raman data. Morse[8] recommends a value of $D_0 = 4(1)$ eV.

F. Group 8

1. Iron

In a density functional calculation, Harris and Jones[96] established that the ground state of iron dimer (Fe_2) is $^7\Delta_u$ from a configuration $(3d\sigma_g)^{1.57}(3d\pi_u)^{3.06}(3d\delta_g)^{2.53}(3d\delta_u)^{2.47}(3d\pi_g)^{2.89}(3d\sigma_u)^{1.49}(4s\sigma_g)^{2.00}$ with a formal bond order of 3. Using EXAFS on matrix-isolated Fe_2, Purdam et al.[97] determined the equilibrium internuclear distance to be $r_e = 2.02$ Å. In matrix isolation Raman studies, Moskovits and DiLella[98] found $\omega_e = 299.6$ cm^{-1} with $\omega_e x_e = 1.4$ cm^{-1}. These numbers were substantiated by negative-ion photoelectron spectroscopy by Leopold and Lineberger.[21,99] A good determination of the dissociation energy has proven more vexing. Lin and Kant[100] used third-law methods to determine a value of 0.78(17) eV. In a later analysis, Haslett, Moskovits, and Weitzman[101] found values in the range of 1.25−1.75 eV. Lian, Su, and Armentrout[102] found a value of 1.14 eV using collision-induced dissociation, and it seems this is the more reliable. Leopold et al.[103] indicate that dissociation is to $4s^23d^6 + 4s^13d^7$ atomic configurations.

In a far-infrared study of the trimer (Fe_3), Nour, Alfaro-Franco, Gingerich, and Laane[104] found vibrational frequencies of $\omega_a = 220$ cm^{-1} and $\omega_e = 180$ cm^{-1}. Haslett et al.[105] in a resonance Raman matrix isolation study found $\omega_a = 249$ cm^{-1} and $\omega_e = 150$ cm^{-1}. Due to the higher resolution and more reliable assignments, we find the latter values more credible. Gutsev, Khanna, and Jena[106] obtained a $^{11}A_1$ ground state, while Castro, Jamorski, and Salahub[107] recommend $^9A_2$. These results imply a C_{2v} geometry

2. Ruthenium

CAS-MCSCF calculations by Das and Balasubramanian[108] as well as SCF−CI calculations by Cotton and Shim[109] indicate that the ground state of ruthenium dimer is $^7\Delta_u$. Resonance Raman matrix isolation[110] studies of mass-selected Ru_2 give $\omega_e = 347.1(9)$ cm^{-1} and $\omega_e x_e = 1.85(15)$ cm^{-1}. Miedma and Gingerich[111] report a value of $D_e = 3.4$ eV.

For the trimer (Ru_3) a mass-selected resonance Raman spectrum[72] yielded only a single progression, presumably the symmetric stretch at $\omega_a = 303.4$ cm^{-1}.

3. Osmium/Iridium

Probably due to their high cost, relatively little spectroscopic information has been obtained for either osmium or iridium clusters. The dissociation energy of Os_2 is $D_0 = 4.3(8)$ eV[8], while for Ir_2 a value of 3.50 eV has been reported.[111] From the rather large dissociation energies, it is likely that strong multiple bonding with large d-orbital contributions exist in these two species. Additional evidence comes from the observation of binuclear complexes such as $Os_2(2\text{-hydroxypyridine})_4Cl_2(C_2H_5)_2O$ for which crystallographic measurements can be obtained. Here the Os−Os internuclear distance is found to be 2.344 Å, indicating a triple bond.[112]

G. Group 9

1. Cobalt

Several calculations[12,113,114] have identified the ground state of cobalt dimer (Co_2) as either $^5\Delta_g$ or $^5\Sigma_g^+$, though it appears the former is more likely. In a mass-selected resonance Raman study in matrix isolation, Dong et al.[115] obtained values of $\omega_e = 296.8(54)$ cm^{-1} and $\omega_e x_e = 2.2(8)$ cm^{-1}, thereby verifying the results of an earlier negative-ion photoelectron spectroscopic study.[21] Using effusion and mass-spectrometric techniques, Kant and Strauss[116] found $D_e = 1.72$ eV, while using collision-induced dissociation (CID) a value of 1.32 eV was obtained.[117] The former value is likely the most reliable.

The ESR of the trimer of cobalt was investigated by Van Zee et al.,[118] who found either $S = 5/2$ or $= 7/2$. Hales et al.[117] found $D_0 = 1.45$ eV as a dissociation energy using CID.

2. Rhodium

In a complete active space SCF calculation including multireference CI, Balasubramanian and Liao[119] indicate that the ground state of rhodium dimer (Rh_2) is $^5\Delta_g$. Wang et al.,[120] using mass-selected resonance Raman spectroscopy, found $\omega_e = 283.9(18)$ cm^{-1} and

$\omega_e x_e = 1.83(33)$ cm^{-1}. Using third-law techniques, Cocke and Gingerich[121] obtained a value of $D_0 = 2.9(2)$ eV, while Langenberg and Morse[122] found $D_0 = 2.4059(5)$ eV using resonant two-photon ionization. This latter value is clearly more reliable, and we adopt it here.

In an ESR study on the trimer (Rh_3), Van Zee et al.[118] found a $^6E'$ (D_{3h}) ground state, while mass-selected matrix isolation resonance Raman spectra[123] indicate $\omega_a = 322.4(6)$ cm^{-1} for a symmetric stretch. The degenerate bending mode is split at 259 and 247.9 cm^{-1}, indicating a slight deviation from equilateral symmetry and an apical angle of 77°. Using the anharmonicity of the totally symmetric stretch ($\omega_a x_a = 0.49(10)$ cm^{-1}), a spectroscopic value of 6.6-(14) eV is obtained for the energy of atomization ($Rh_3 \rightarrow 3Rh$). Using photolytic dissociation in matrix isolation, Ozin and Hanlin[124] obtain a value for the dissociation energy ($Rh_3 \rightarrow Rh_2 + Rh$) of 4.16 eV. Combined with the dimer dissociation energy of 2.05 eV, an independent measure of the atomization energy of 6.21 eV is obtained, in reasonable agreement with the spectroscopic results.

3. Iridium

See discussion for osmium.

H. Group 10

1. Nickel

Two studies of gas-phase jet-cooled nickel dimer[125,126] (Ni_2) have been carried out concluding that the ground state is 0_g^+ ($^3\Sigma_g^- + {}^1\Sigma_g^+$), with several low-lying states (0_u^- at 12 cm^{-1} and 5_u at 58 cm^{-1}) and $r_e = 2.1545(4)$ Å. The authors also report $D_0 = 2.068(2)$ eV. In a mass-selected resonance Raman study, Wang et al.[127] obtained $\omega_e = 259.2(30)$ cm^{-1} and $\omega_e x_e = 1.9-(7)$ cm^{-1}. These results indicate that the bond in Ni_2 is relatively weak, comparable to Cu_2, and that there is little, if any, contribution of the d electrons to bonding. This is likely due to the contracted nature of the 3d electrons and more diffuse 4s shell.

The trimer of nickel (Ni_3) has been the subject of a far IR study by Nour et al.[104] as well as a resonance Raman matrix isolation study by Moskovits and DiLella.[128] The results indicate that the symmetric stretch is $\omega_a = 232$ cm^{-1} and the asymmetric stretch is at 198 cm^{-1}. A normal-mode analysis of the spectra indicates C_{2v} symmetry with a bond angle of 90−100°, assuming a ratio of stretch−stretch force constant (f_{rr}) to stretch (f_r) interaction of 0.05.

2. Palladium

Ho, Polak, Ervin, and Lineberger[129,130] in a photoelectron spectroscopy study of palladium dimer (Pd_2) show that the ground state is $^3\Sigma_u^+$. The ground state of the Pd atom ($4d^{10}5s^0$) is not conducive to good bonding due to the filled d and empty s orbitals, and since the dimer ground state is $^3\Sigma_u^+$, good bonding likely requires promotion of two atoms to $4d^95s^1$ (^3D, with promotion energy of 0.407 eV each), contributing to a $(4d\sigma_u)^1(5s\sigma_g)^1$ configuration. Their value for the vibrational frequency is $\omega_e = 210(10)$ cm^{-1}. Shim and Gingerich[131] report a value of $D_0 = 1.03(16)$ eV for the dissociation energy. This is in agreement with the second-law value of $D_0 = 1.1(1)$ eV of Lin, Strauss, and Kant.[132]

Ervin, Ho, and Lineberger[133] obtained a negative-ion photoelecton spectrum of the trimer of palladium but observed no vibrational resolution.

3. Platinum

There are three different measures of the ground-state vibrational frequency of platinum dimer. The earliest was from a photoelectron spectrum by Ho, Polak, Ervin, and Lineberger[134] in which $\omega_e = 215(15)$ cm^{-1}. Using jet-cooled dispersed fluorescence, Pinegar et al.[135] found a value of 222.5(7) cm^{-1}, and in a mass-selected luminescence spectrum,[136] 197.4(33) cm^{-1} was obtained. These values do not disagree too much, but the disagreement is greater than is likely from matrix effects alone. It should be pointed out that in none of the experiments could it be definitely established that the ground state has been observed. Taylor and Lemire et al.[137], in a resonant two-photon ionization study of jet-cooled Pt_2, found an accurate value of $D_0 = 3.14(2)$ for the dissociation energy. In principle, all three observations of the vibrational frequency may be in different states. The values are all similar, if not within experimental error. We take the result of 222.5 cm^{-1} since it is the most accurate gas-phase result. This gives a force constant of 2.84 mdyne/Å. Cui et al.[138] and Balasubramanian[139] agree with separate calculations that the ground state is $^3\Sigma_g^-$ (0_g^+). In a rotationally resolved high-resolution study of laser-induced fluorescence, Airola and Morse[140] obtained an internuclear distance of $r_0 = 2.33297(33)$ Å in the ground state, which they indicate is most likely 0_g^+. This short internuclear distance (0.14 Å shorter than that of Au_2) is taken as strong evidence of substantial 5d participation in the chemical bond.

The only measurement of the trimer of platinum is in a study of the photoelectron kinetic energy of the anion produced in a flowing afterglow ion source, excited by a cold cathode dc discharge.[141] Progressions in 225(30) cm^{-1} and 105(30) cm^{-1} were obtained and assigned to the symmetric stretch and degenerate bend of the neutral trimer. It is unlikely that two so disparate values are both symmetric stretches of two different electronic states. Note that if this assignment is correct, the rather large deviation of the ratio of the two frequencies from $2^{1/2}$ indicates that there is a substantial deviation from D_{3h} symmetry. Kua and Goddard[142] show, using density functional theory, that in the equilateral triangle geometry the ground state of the trimer is most likely a triplet.

I. Group 11

1. Copper

Numerous experimental studies have been carried out for the dimer of Cu,[143−148] but we will only discuss the most recent, which is perhaps the most accurate. Ram, Jarman, and Bernath,[149] in a remarkable study, obtained a gas-phase Fourier transform emission spectrum of Cu_2. For the $^1\Sigma_g^+$ ground state, they

obtained $\omega_e = 266.4594(29)$ cm^{-1} and $\omega_e x_e = 1.0350(16)$ cm^{-1}. The equilibrium internuclear distance $r_e = 2.21927(3)$ Å. The dissociation energy is $D_0 = 2.03$ eV.[150]

Considerable attention has been paid to the copper trimer (Cu_3).[151−160] Virtually all authors agree that the ground state is $^2E'$ (D_{3h}), which is distorted by Jahn−Teller effects leading to either $^2A_1$ or $^2B_2$ in C_{2v}. Rolfing and Valentini[151] obtained a laser-excited fluorescence spectrum of jet-cooled Cu_3 and obtained over 30 bands from two levels of an excited $^2E''$ state. In two independent analyses[154,153] most of these bands were fit using a large barrier to pseudorotation. The results were $\omega_a = 269.5$ cm^{-1}, $\omega_e = 137$ cm^{-1}, $k = 1.86$, and $g = 0.223$. The last two are the linear and quadratic Jahn−Teller parameters, respectively. However, there are some difficulties with this assignment. In addition to lack of complete assignment of all observed lines, the trimer symmetric stretch frequency is higher than that of the dimer. Though not impossible, this is at least unusual. In Appendix A, we propose an alternative assignment which not only fits all observed lines but does so with a smaller standard deviation and with the use of only three adjustable parameters instead of four. The results are $\omega_a = 230$ cm^{-1}, $\omega_e = 145$ cm^{-1}, and $\alpha = 8.07$; the latter is the coefficient for pseudorotation (see Appendix A). Both fits suffer from an inability to predict correctly the intensities of several lines. In the absence of further evidence, we feel it is impossible at this point to choose between these alternatives and thus report both values for our discussion.

2. Silver

The clusters of silver are perhaps the most widely studied. This is because the sputtering mass spectrum of silver is quite extensive[161] with stable clusters detected up to Ag_9, allowing unambiguous mass selection for several cluster sizes. Except for the dimer, the sputtering mass spectrum of Ag is dominated by odd clusters so that most of the Raman work is on these clusters only.

The dimer was originally investigated in the gas phase by Srdanov and Pesic[162] and later by Brown and Ginter.[163] They report a $^1\Sigma_g^+(O_g^+)$ ground state with $\omega_e = 192.4(5)$ cm^{-1} and $\omega_e x_e = 1.55(5)$ cm^{-1}. Furthermore, from a rotational analysis a value of $r_0 = 2.469$ Å was obtained. However, several more recent measurements report a value of $r_0 = 2.53350(48)$[164] and 2.5303(2) Å[165]. We take these latter values to be the best. The dissociation energy of $D_e = 1.65(3)$ eV has also been reported.[8]

Silver trimer provides considerably more ambiguous results. The ground state is most likely a Jahn−Teller-distorted $^2E'$ (D_{3h}) state, which is split into $^2B_2$ and $^2A_1$ states in C_{2v} symmetry. In a very convincing study utilizing mass selection, Haslett, Bosnick, Fedrigo, and Moskovits[166] use matrix isolation resonance Raman spectroscopy to obtain $\omega_a = 119$ cm^{-1} for the totally symmetric mode and $\omega_e = 99$ cm^{-1} for the degenerate bend. This is in agreement with Schulze and Becker,[167] who obtained 120.5 cm^{-1} in matrix isolation, but somewhat different from Okazake et al.,[168] who obtained $\omega_a = 138.8(10)$ cm^{-1}(for $^{107}Ag_3$) using optical emission in the gas phase. However, their spectral lines are weak, on a broad and variable background, and somewhat congested. Thus, this gas-phase assignment must be regarded as questionable.

In contrast with these studies is a supersonic molecular beam pulsed-nozzle laser vaporization experiment by Cheng and Duncan.[169] Using mass-resolved two-photon ionization, there is no doubt as to the species involved and the vibronic spectra are clear and sharp. The spectra can be fit assuming a weak Jahn−Teller distortion and vibrational frequencies of $\omega_a = 161.1$ cm^{-1} for the totally symmetric mode and $\omega_e = 96.3$ cm^{-1} for the degenerate bend. Later Wedum et al.[170] reinterpreted this spectrum incorporating a more careful theoretical analysis as well as extended experimental results. Wallimann et al.[171] also conducted pulsed-nozzle jet-cooled supersonic expansion experiments with resonant two-photon ionization (R2PI) observing spectra up to 1000 cm^{-1} above the origin. They utilized both Jahn−Teller and spin−orbit effects to analyze the spectrum with $\omega_a = 157.9$ cm^{-1} for the totally symmetric mode and $\omega_e = 140.0$ cm^{-1} for the degenerate bend. Their Jahn−Teller parameters differ considerably from those obtained by Wedum et al.[170] In another study of dispersed fluorescence, Ellis, Robles, and Miller[172] obtained values of $\omega_a = 180$ cm^{-1} for the totally symmetric mode and $\omega_e = 67$ cm^{-1} for the degenerate bend. Although these three values do not agree exactly, the first two are quite close, and given their inherently higher resolution, we take the value of 157.9 cm^{-1} as most likely representative.

There thus seems to be a conflict between the gas-phase studies and the matrix isolation studies, despite the fact that both experiments use some form of mass selection. It is difficult to reconcile these two views, since normally matrix effects on vibrational frequencies are usually small, often less than 1%. Since Ag has a filled d shell, we do not expect the large number of low-lying states produced by unfilled d orbitals, which is common in other transition-metal clusters. Thus, we cannot readily explain the discrepancy by preferential matrix stabilization of a low-lying excited state. For our purposes here, we wish to establish a force constant in silver trimer, but it is difficult to choose between the two possible values. However, the gas-phase value is more consistent with spectra obtained in larger clusters (see section VI, below), and we utilize that value in calculating the trimer force constant for Table 6.

The fluorescence and excitation spectrum of mass-selected Ag_4 has been obtained by Felix et al.[173] A peak at 458 nm was obtained, but lack of vibronic resolution resulted in no vibrational constants for the ground state. Unresolved fluorescence has also been observed in Ag_8 near 321 nm in argon matrices and droplets.[174]

Haslett, Bosnick, and Moskovits[175] investigated the matrix isolation Raman spectrum of mass-selected Ag_5 and concluded that its structure is that of a planar trapezoid. Vibrational bands were obtained at 68, 80, 100, 105, 126, 136, and 174 cm^{-1}. In

addition, a strong progression originating at 162 cm^{-1} was obtained, with overtones at 323 and 486 cm^{-1}. The bands at 100 and 105 cm^{-1} were interpreted as a single vibration split by matrix effects. So many distinct fundamentals are indicative of low symmetry for a pentamer, and the highest possible symmetry was assumed to be C_{2v}. Any higher symmetry geometry would lead to many less distinct fundamentals. Since lower symmetry requires more force constants, several assumptions were required as to the likely magnitude of these parameters in carrying out normal coordinate calculations. With reasonable assumptions, various likely geometries were compared. The planar trapezoid geometry was suggested by several calculations, and this geometry best fit the observed spectrum.

Resonance Raman spectra of mass-selected Ag_7 and Ag_9 have been obtained by Bosnick, Haslett, Fedrigo, and Moskovits.[176] They found that both the heptamer and nonamer spectra are dominated by a totally symmetric breathing mode band at 165 cm^{-1}. The heptamer could be interpreted as a tricapped tetrahedron, while no structural inferences could be made concerning the larger cluster. However, these frequencies are quite close to the Debye frequency of solid silver (156 cm^{-1}), implying that bonding in clusters of this size already approximates that of the bulk.

Support for this view comes from studies of the optical absorption of size-selected clusters (n = 5, 7, 8, 9, 11) embedded in argon matrices by Harbich and co-workers.[177,178] The absorption between 3 and 4 eV shows between one and three peaks, depending on cluster size, and could be fit with a simple Drude model using only s electrons.

3. Gold

In a high-resolution gas-phase spectroscopic study of gold dimer (Au_2), Ruamps[179] found that the ground $^1\Sigma_g^+(0_g^+)$ state could be characterized by vibrational frequencies of $\omega_e = 190.9$ cm^{-1} and $\omega_e x_e = 0.420$ cm^{-1}. Simard and Hackett[180] used high-resolution rotational spectroscopy to obtain $r_e = 2.4715$ Å, while a dissociation energy $D_0 = 2.290(8)$ eV was obtained by a jet-cooled resonant two photon ionization study by Bishea and Morse.[181]

Gold trimer (Au_3) was studied by ab initio calculations[182] to have a $^2E'$ (D_{3h}) ground-state distorted by Jahn−Teller interactions to $^2B_2$. Although no ground-state vibrational frequency was obtained, $\omega_a = 179.9$ cm^{-1} was observed by Bishea and Morse[183] for an excited $^4E'$ state. They found the dissociation energy (Au_2−Au) to be 1.51(15) eV and the atomization energy to be 3.80(13) eV.

J. Group 12

1. Zinc/Cadmium/Mercury

With filled atomic orbitals ($d^{10}s^2$) we expect only weak van der Waals bonding in the dimers of zinc, cadmium, and mercury. Gas-phase laser-induced fluorescence studies were carried out on jet-cooled Cd_2 and Zn_2 by Czajkowski and Koperski.[184] For both species they found a $^1\Sigma_g^+$ (O_g^+) ground state. For Zn_2, they obtained $\omega_e = 25.9(2)$ cm^{-1}, $\omega_e x_e = 0.60(5)$ cm^{-1}, $D_e = 0.03$ eV, and $r_e = 4.19$ Å. For Cd_2, they obtained $\omega_e = 23.0(2)$ cm^{-1}, $\omega_e x_e = 0.40(1)$ cm^{-1}, $D_e = 0.041$ eV, and $r_e = 4.07$ Å.

For the dimer of mercury (Hg_2), van Zee, Blankespoor, and Zwier[185] found a $^1\Sigma_g^+$ (0_g^+) ground state with $\omega_e = 18.5(5)$ cm^{-1}, $\omega_e x_e = 0.27(1)$ cm^{-1}, $D_e = 0.043$ eV, and $r_e = 3.63(4)$ Å. Their dissociation energy was obtained by using the spectroscopic anharmonicity $D_e = \omega_e^2/4\omega_e x_e$, while Hilpert[186] reports a value of $D_e = 0.074(20)$ eV. Koperski, Atkinson, and Krause[187] carried out a supersonic jet dye laser excitation spectrum from which the obtain $\omega_e = 19.9(5)$ cm^{-1} and $\omega_e x_e = 0.26(1)$ cm^{-1} in substantial agreement with previous results.

Clearly these values are consistent with the expected extremely weak bonding. Yu and Dolg examined possible small contributions of covalent bonding[188] to these dimers with relativistic pseudopotentials in a coupled cluster calculation, which reproduces the spectroscopic constants quite well.

IV. Transition-Metal Dimers

A. Force Constants

With the vibrational frequencies (ω_e) obtained in the various experiments, we are now in a position to calculate values of the force constants. For dimers, we use the formula $k_e = {}^1/_2 m\omega_e^2$ where m is the isotope-abundance-weighted atomic mass, unless sufficient spectroscopic resolution is obtained to resolve isotopic lines, in which case the appropriate isotopic mass is used. The conversion factor is 1 amu $cm^{-2} = 5.8919 \times 10^{-7}$ mdyne/Å. In Table 1 we list the dimer force constants obtained from the experimental frequencies. The values shown for Tc_2, Os_2 and Ir_2 in parentheses were not obtained from spectroscopic frequencies but from a fit of the force constants to diabatic dissociation energies, which is discussed in section IV.C below.

One of the goals of this research is to help understand the nature of bonding in metal clusters. In the transition metals, bonding is dominated by the s and d electrons. The extent of the d-orbital contribution to bonding varies considerably throughout each transition-metal series. It is largely dependent on the relative availability for bonding of the (n + 1)s electrons as compared with that of the nearly isoenergetic (n)d electrons. The ratio of the expectation value of the orbital radii $<r_{(n)d}>/<r_{(n+1)s}>$ is found to decrease considerably with increasing atomic number within a particular transition-metal row. Both (n)d and (n + 1)s orbitals contract as the nuclear charge increases, but the (n)d electrons are not shielded as effectively as the (n + 1)s electrons and therefore contract more rapidly. Thus, d electrons tend to be spatially less available for chemical bonding in the late transition metals.

In addition to spatial extent, we must also examine energetic considerations. Many transition-metal atoms possess ground d^ms^2 configurations. These are unsuitable for covalent bonding since the s orbital is filled. In order for a good bond to form between two metal atoms, at least one must be promoted to the

Table 1. Ground-State Dimer Force Constants (in mdyne/Å) for Transition Metals[a]

Sc_2	Ti_2	V_2	Cr_2	Mn_2	Fe_2	Co_2	Ni_2	Cu_2	Zn_2
0.76	2.35	4.33	3.54	0.09	1.48	1.53	1.16	1.33	0.01
Y_2	Zr_2	Nb_2	Mo_2	Tc_2	Ru_2	Rh_2	Pd_2	Ag_2	Cd_2
0.89	2.51	4.84	6.33	(4.37)	3.59	2.44	1.38	1.18	0.02
Lu_2	Hf_2	Ta_2	W_2	Re_2	Os_2	Ir_2	Pt_2	Au_2	Hg_2
0.76	1.63	4.80	6.14	6.26	(6.26)	(4.44)	2.84	2.12	0.02

[a] Metals in red were studied in mass-selected experiments. Those in green were estimated from a fit of force constants and diabatic dissociation energies.

$d^{m+1}s^1$ configuration. The resulting bond strength is consequently reduced by the promotion energy required. Still further complications ensue when relativistic considerations are taken into account. The effects of relativity[189,190] increase dramatically with increasing nuclear charge and therefore display more influence in the third row of transition elements as well as the lanthanides. Orbitals that have significant density near the nucleus (especially s orbitals)[191] show an increased contraction, while d and f orbitals tend to be relatively less effected. The latter are better shielded than the more contracted s orbitals, making them more available for bonding. This relativistic effect makes the 6s orbital of gold smaller and less diffuse than the corresponding 5s orbital in silver. Thus, gold dimer has a shorter bond length and a larger vibrational frequency and dissociation energy than silver dimer.[192,193] Third-row species also involve possible contributions from f orbitals, although it is usually stated that their contributions are slight, since the f electrons are more closely bound to the nucleus than the valence d or s electrons. However, in the lanthanide series, indirect effects are observed.

We therefore seek to determine the extent to which the observed force constants enable us to obtain information as to the extent of d-orbital contribution to the chemical bond as we cross the periodic table. The force constant is defined as the second derivative of the potential curve at the equilibrium internuclear distance.

$$k_e = \left(\frac{\partial^2 V}{\partial r^2}\right)_{r=r_e}$$

The force constant is thus sensitive to the strength of chemical bonding near equilibrium. Pauling's rule[194,195] makes this more explicit. Pauling showed that the force constant is approximately proportional to the bond order. Thus, the force constant is a direct measure of the number of electrons that contribute to a bond, and ratios of force constants are good measures of relative bonding strength. By comparing force constants across a transition-metal series, we may obtain a direct measure of the degree to which additional d electrons contribute to the bond strength. We may take advantage of Pauling's rule by recognizing that dimers of species with an atomic configuration $d^{10}s^1$ (i.e., the coinage metals) have filled d shells that preclude the participation of d electrons in bonding. In these dimers bonding is likely to be close to that of a pure single bond. If we then take the ratio of the force constant for each dimer in a row to that of the last member (i.e., coinage metal), we obtain a direct measure of the effect of varying d electrons on the dimer bond. This is illustrated in Figure 2, where we plot bond order for all the dimers of the transition metals in this way. Note that the term "bond order" as used here is not the same as the usual chemical definition [i.e., $^1/_2$(no. of bonding electrons − no. of antibonding electrons) or better a function of the electron density]. This might more accurately be termed the "vibrational bond order" since it is experimentally determined. For brevity, we shall use just "bond order" in this work, except where a distinction must be made.

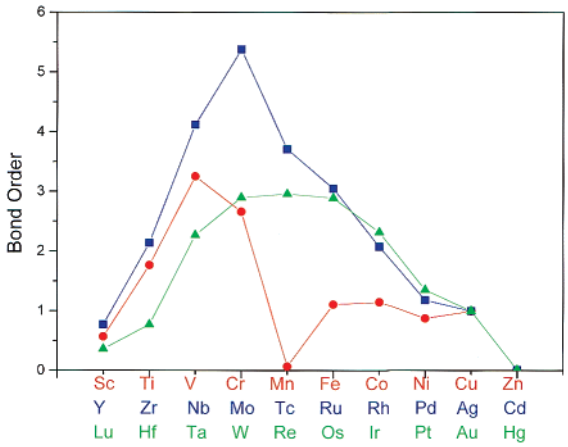

Figure 2. Vibrational bond orders of transition-metal dimers. Bond orders for each row of the periodic table are obtained from force constants using Pauling's rule by taking the ratio of force constant to that of the coinage metal dimer in the corresponding row. It is assumed that the bond order for the coinage metal dimers is one. Circles are for the first row, squares for the second row, and triangles for the third row.

For the first row, the bond order initially increases sharply up to over three for V_2, indicating successive increases in the number of d electrons available for forming a chemical bond. However, for Cr_2 and Mn_2 the bond order decreases to near zero for the latter, indicating van der Waals bonding due to the special stability of a half-filled d-shell ($3d^54s^1$ for Cr and $3d^5$-$4s^2$ for Mn). This aversion to bonding is not mitigated by 4s → 3d promotion since the energetic cost of such

a promotion is too high. These effects continue to be felt through the remainder of the row for Fe_2, Co_2, and Ni_2. Small contributions from d electrons are apparent in Fe_2 and Co_2 with bond orders only slightly greater than one. Presumably, the relative contraction of the 3d orbital in the late transition series results in a severely diminished force constant. Nevertheless, it is likely that in these two dimers at least one 4s → 3d promotion is achieved due to the relatively low energetic cost (0.87 and 0.43 eV, respectively). In Ni_2, the relatively low bond order, below even that of Cu_2, indicates complete lack of d-electron contribution to the bond.[127]

Examining bond orders for the second row we observe a steady increase from Y_2 through Mo_2, which has perhaps the highest bond order (5.5) of any known chemical bond. Despite the half-filled d orbital ($4d^55s^1$) for Mo, it is apparent that all the d electrons make important contributions to the bonding. After Mo, there is a steady decrease due to the decreasing 4d−4d orbital overlap between centers along with the increasing number of electrons occupying antibonding orbitals.

In the third row we see the same pattern as the second row but with relatively lower bond orders. The half-filled d orbital in Re ($5d^56s^2$) does not interfere with d-orbital bonding in the dimer, which has a bond order near three. This is in marked contrast to Mn_2, which is merely bound by van der Waals bonding. Manganese dimer perhaps has the weakest of the dimer bonds. This is best explained by the ratio $\langle r_{5d}\rangle/\langle r_{6s}\rangle$ for Re which is 0.570 while for Mn $\langle r_{3d}\rangle/\langle r_{4s}\rangle = 0.351$. Hence, there is a possibility of much stronger overlap between d electrons in Re than in Mn. Furthermore, the rather large s−d promotion energy in Mn militates against formation of even a strong 4sσ bond. Unfortunately, due to radioactivity and cost, spectroscopic studies have not been carried out in technetium dimer (Tc_2). It would be of considerable interest to determine whether Tc_2 behaves more like Mn_2 or Re_2. The ratio of $\langle r_{4d}\rangle/\langle r_{5s}\rangle = 0.474$ indicates substantial opportunity for d-orbital participation, suggesting that bonding will be considerably stronger in Tc_2 than in Mn_2 but not as large as in Re_2. Across the third row there is sufficient energy obtained from the formation of chemical bonds to overcome even relatively large 6s → 5d promotion energies, so that it is likely that these species dissociate with at lease one excited state atom. This, plus the relatively larger extent of d-orbital radius, allows for maximum participation of d electrons in bonding, and this is reflected in the smooth, almost symmetric plot of bond order for the third row.

B. Dissociation Energies

Another important measure of the strength of chemical bonds is the adiabatic dissociation energy (D_e), which represents the difference in energy between the minimum of the potential energy curve and the dissociation limit. Dissociation energies are good measures of bond strengths in that they are sensitive to the entire range of the potential curve, from its minimum to asymptote, and therefore have considerable thermodynamic utility. They are closely related to the thermodynamic enthalpy for the dissociation reaction $A_2 = 2A$, and may be determined by second- or third-law methods.[196] These involve Knudsen effusion mass-spectrometric techniques. Such measurements have the advantage of being relatively easy to carry out and generally applicable. Thus measurements of almost all dimer dissociation energies have been obtained by this method. However, there are some difficulties with this technique.[122] One is that for the third-law technique the absolute entropy of the diatomic transition metal must be calculated, and this requires ground-state internuclear distances and frequencies as well as parameters for low-lying electronic states. These are often not known accurately and must be estimated.

Another possible way to measure dissociation energies involves determination of the anharmonicity ($\omega_e x_e$) of the potential curve spectroscopically. This is carried out in practice by measuring the deviation from regular spacing of the bands in a vibrational progression. Assuming a Morse potential, the dissociation energy is then obtained by the formula

$$D_e = \frac{\omega_e^2}{4\omega_e x_e}$$

This spectroscopic technique also presents difficulties. First, the anharmonicity is often poorly determined. The relative error is often large, resulting in a large relative error in D_e. In addition, for transition metals, with contributions to the bonding from both s and d electrons, the potential curve may deviate considerably from a Morse potential. This is due to the sharply differing spatial extent of s and d orbitals, resulting in separate rates of dissociation with increasing internuclear distance. Such an effect shows clearly in the observed vibrational levels of Cr_2 in which anharmonic corrections up to sixth order are required for an adequate fit.[76] The potential energy curve includes a shelf-like shoulder, creating large discrepancies in the various measures of bond strength. Due to severe difficulties with this method, we do not utilize these spectroscopic determinations of D_e in our discussion of dimer dissociation.

Perhaps the most accurate and reliable method for determining dissociation energies involves observation of an abrupt predissociation threshold in a resonant two-photon ionization spectrum of jet-cooled dimer. The technique, pioneered by Morse and coworkers,[122] is capable of accuracies up to 0.02%. Unfortunately this method is not universally applicable to all dimers.

The widely varying methods for measuring dissociation energies sometimes leads to considerable difficulty in deciding which result to use. For example, in iron dimer, values as different as 0.78 and 1.75 eV have been reported. In our discussions below we use the predissociation threshold values where they have been obtained and otherwise use results of the thermodynamic experiments.

C. k_e vs D_e Correlation

We now have two measures of bond strengths, both of which have been obtained for most if not all of the

Table 2. Ground-State Transition-Metal Dimer Term Symbols, Dimer Adiabatic Dissociation Energies (eV), Atomic Promotion Energies (eV), and Dimer Diabatic Dissociation Energies (eV)[a]

Sc_2	Ti_2	V_2	Cr_2	Mn_2	Fe_2	Co_2	Ni_2	Cu_2	Zn_2
$^5\Sigma_u^-$	$^3\Delta_g$	$^3\Sigma_g^-$	$^1\Sigma_g^+$	$^1\Sigma_g^+$	$\{^7\Delta_u\}$	$\{^5\Delta_u\}$	0_g^+	$^1\Sigma_g^+$	$^1\Sigma_g^+$
1.65	1.4	2.75	1.44	0.1	1.12	1.72	2.068	2.03	0.03
1.43	0.81	0.25	0	2.14	0.87	0.42	0	0	---
3.08	3.02	3.25	1.44	0.1	1.99	1.72	2.068	2.03	0.03

Y_2	Zr_2	Nb_2	Mo_2	Tc_2	Ru_2	Rh_2	Pd_2	Ag_2	Cd_2
$^5\Sigma_u^-$	$^3\Delta_g$	$^3\Sigma_g^-$	$^1\Sigma_g^+$	---	$\{^7\Delta_u\}$	$\{^5\Delta_{g,u}\}$	$\{^3\Sigma_u^+\}$	$^1\Sigma_g^+$	$^1\Sigma_g^+$
1.62	3.052	5.48	4.48	3.42	3.4	2.405	1.03	1.65	0.041
1.36	0.59	0	0	0.41	0	0	0.407	0	---
2.98	4.13	5.48	4.48	4.24	3.4	2.405	1.84	1.65	0.041

Lu_2	Hf_2	Ta_2	W_2	Re_2	Os_2	Ir_2	Pt_2	Au_2	Hg_2
$\{^5\Sigma_u^-\}$	---	---	$\{^1\Sigma_g^+\}$	$^3\Delta_g$	---	---	0_g^+	$^1\Sigma_g^+$	$^1\Sigma_g^+$
1.43	3.4	4	5	4.44	4.3	3.5	3.14	2.29	0.043
2.34	1.69	1.04	0	1.76	0.75	0.40	0	0	---
3.77	6.8	4	5	6.20	5.80	4.30	3.14	2.29	0.043

[a] The promotion energies for each atom is the difference in energy between the lowest spin−orbit level deriving from a $d^n s^1$ configuration and the ground level. The term symbols in brackets {} are theoretical and have not been confirmed experimentally. The 0_g^+ symbols for Ni_2 and Pt_2 are derived from strong spin−orbit mixing of $^3\Sigma_g^-$ and $^1\Sigma_g^+$ states.

transition-metal dimers, and it would therefore be of interest to see the extent to which they are comparable. We have attempted to plot measured values of the dimer force constants against measured values of the dissociation energies. However, the scatter is so great that reasonable fits were of no value. We have found that if instead we use diabatic dissociation energies, a much better correlation is obtained. Diabatic dissociation energies can be obtained from the adiabatic dissociation energies, where needed, by adding either the s→d promotion or twice that to take into account the additional energy needed for formation of a strong chemical bond. Referring to experimental evidence described above (see section III) concerning the atomic configuration to which the dimers dissociate, for Ti_2, V_2, Zr_2, and Pd_2 we have used twice the promotion energy (Note, we have also done this for Tc_2, Hf_2, Os_2, and Ir_2, but the experimental evidence to justify this is weak), while for the dimers Sc_2, Fe_2, Y_2, Lu_2, and Re_2 we have assumed only a single excited atom on dissociation. This data is collected in Table 2. In our correlation, we have excluded all dimers that have bond orders less than one, as possibly being too weakly bonded for a valid comparison. We have also excluded Cr_2, due to the severely distorted potential curve, and Hf_2, since the reported dissociation energy is unreliable. We show the plot of dimer force constants (k_e) vs diabatic dissociation energies (D_e^d) in Figure 3. An excellent fit can be obtained to a straight line of the form $k_e = 1.21D_e^d - 0.76$ with a correlation coefficient of 0.9. It is clear, then, that both measures of bond strength are comparable if proper account of promotion energy is taken.

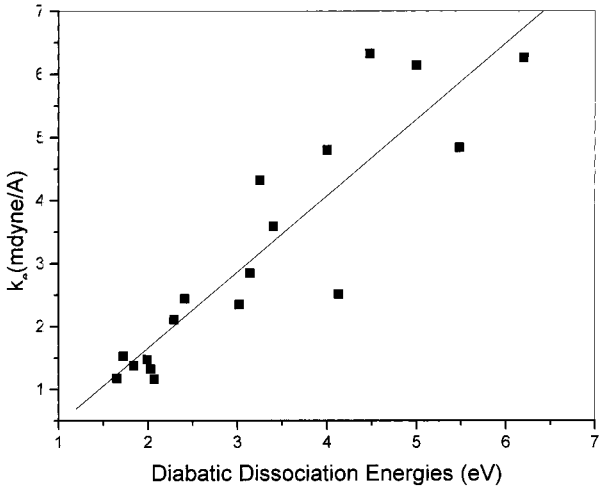

Figure 3. Plot of experimental transition-metal dimer force constants (mdyne/Å) vs diabatic dissociation energies (eV). The straight line represents the linear regression best fit to the observed data.

We may also use this fit to obtain estimates of the force constants for the three species in which measurements could not be obtained. For Tc_2 we obtain

$k_e = 4.37$ mdyne/Å, while for Os_2 and Ir_2 we obtain 6.26 and 4.44 mydne/Å, respectively. We have included these values in the above bond order plots, and it can be seen that they fit quite well with the trends observed. This is especially satisfying for Tc_2, which clearly has a strong chemical bond, with a bond order of nearly 3.5. This is in fact just slightly lower than would be predicted by interpolating a straight line in the second-row bond order plot (Figure 2). It also shows that bonding in Tc_2 is more nearly like that of Re_2 than Mn_2, as predicted above by consideration of the value of $<r_{4d}>/<r_{5s}>$. In the third row, the inclusion of Os_2 and Ir_2 force constants in the plot results in an almost symmetric curve about the row center.

D. Ground-State Term Symbols

In Table 2, in addition to dissociation energy information, we have included, where known, term symbols for dimer ground states. Those listed in brackets ,{}, are suggested by theoretical calculations but not experimentally verified. In most of the entries we have used case a notation for uniformity of presentation. However, for Ni_2 and Pt_2 there is clear evidence for strong spin−orbit coupling in the ground $^3\Sigma_u^+$ state to require a case c 0_g^+ assignment. It is reasonable that Pd_2 will show a similar result, but at present there is no experimental evidence for this. With these considerations in mind, it is worthwhile examining some of the patterns observed in this table. First we notice that except for the fifth column, all the term symbols are the same in a vertical column. The exception is for Mn_2, which is expected since it is a van der Waals complex and thus differs considerably in binding properties from Tc_2 and Re_2, as discussed above. The second observation is that all states are either Σ or Δ, indicating that total orbital angular momentum about the nuclear axis (Λ) is either 0 or 2. No Π ($\Lambda = 1$) states are observed. If we imagine that each series is broken up into two half-periods (1−5 and 6−10) we see that for each half-period the second dimer has Δ symmetry. By examination of the molecular orbital configurations which lead to these terms (see section III above), it can be seen that for all those species with Δ terms there is an odd number of electrons in a δ orbital. The other pattern that emerges is that for each half-period the spin degeneracy starts high (quintet or heptet) and steadily drops across the half-period. Once again, the exception may be in the fifth column where Re_2 has a $^3\Delta_g$ state. In any case, it is clear that as each half-period is filled, spins tend to be paired more strongly.

E. Internuclear Distances

To determine accurate ground-state internuclear distances it is necessary to obtain good gas-phase, rotationally resolved spectra either in absorption or emission. This is often difficult either due to broad line widths or narrow rotational spacings. The latter is especially a problem for the heavier dimers of the third row of the transition metals or lanthanides, since their rotational spacings tend to be even closer than the Doppler width, making it impossible to resolve rotational structure using normal spectroscopic means. As a consequence, the number of dimers for which accurate equilibrium internuclear distances have been obtained is considerably more limited than those for which force constants have been measured. Nevertheless, we have collected the results that have been obtained and display them in Table 3. In the first rows just below the metal symbol are the experimental values in Å.

Table 3. Ground-State Dimer Internuclear Distances (Å)

Sc	Ti	V	Cr	Mn	Fe	Co	Ni	Cu	Zn
	1.942	1.77	1.679	3.4	2.02		2.154	2.22	4.19
2.46	1.97	1.71	1.80	3.37	2.17	2.16	2.28	2.22	4.22
Y	Zr	Nb	Mo	Tc	Ru	Rh	Pd	Ag	Cd
	2.24	2.078	1.929					2.53	4.07
2.62	2.28	2.07	1.98	2.10	2.17	2.29	2.48	2.53	4.03
Lu	Hf	Ta	W	Re	Os	Ir	Pt	Au	Hg
							2.33	2.47	3.69

There are certainly enough results displayed to make it worthwhile to examine whether correlations exist between these results and other properties. The most famous correlation expected is that of Badger's Rule,[197] an empirical rule, which states that there is an inverse correlation between the force constant and the third power of the internuclear distance. This may be written

$$k_e(r_e - d_{ij})^3 = C$$

where C is a universal constant and d_{ij} is a constant which depends on the rows of the periodic table from which each atom of the diatomic molecule resides. A valuable review has been presented by Herschbach and Laurie.[198] Weisshaar applied this rule to third-row metal diatomics.[199] Although this rule has found considerable application in various branches of chemistry, it has been found to be accurate only to 15−20%.[200]

Another empirical correlation between bond length and force constant has been explored by Guggenheimer.[201] He showed that

$$k_e = c(z_1 z_2)^{1/2} r_e^{-2.46}$$

where z_1 and z_2 are the number of *s*- and *p*-valence electrons contributed to the bond from each atom and c is a constant. This provides a considerably better fit than Badger's rule but does not provide clear guidance as to how to include d electrons in the correlation. Instead we turn to an empirical relationship obtained by Pauling[194] between crystal lattice constants and bond order. It is worthwhile to determine the applicability of this relationship to transition-metal dimers. This is especially convenient in that we have determined experimental bond orders for all the transition-metal dimers (see Figure 2). Pauling's relationship may be written

$$R_n = R_1 - b_{ij} \log(n)$$

R_n is the internuclear distance when the bond order is n, R_1 is the internuclear distance for a single bond,

Table 4. Configuration of Atomic Ground State, Promotion (6s→5d) Energies (eV), Atomic Radii (pm), Ionic (3+) Radii (pm), Ratio of Relativistic to Nonrelativistic 6s and 4f Orbital Radial Expectation Values, Dimer Dissociation Energies D_0 (eV), Diabatic Dissociation Energies D_0^d (eV), Ground-State Vibrational Frequencies ω_e (cm^{-1}), Force Constants k_e (mdyne/Å), and Dimer Ground-State Term Symbols of Lanthanides[a]

element	La	Ce	Pr	Nd	Pm	Sm	Eu	Gd	Tb	Dy	Ho	Er	Tm	Yb	Lu
configuration($6s^2$)	$5d^1$	$4f^15d^1$	$4f^3$	$4f^4$	$4f^5$	$4f^6$	$4f^7$	$4f^75d^1$	$4f^9$	$4f^{10}$	$4f^{11}$	$4f^{12}$	$4f^{13}$	$4f^{14}$	$4f^{14}5d^1$
P.E. (6s→5d)	0.33	0.29	1.01	1.05		1.34	1.6	0.79	1.87	2.17	2.34	2.4	2.53	3.04	2.34
atomic radius	187	183	182	181	181	180	199	179	176	175	174	173	173	194	172
ionic (3+) radius	107	103	101	99		96	95	94	92	91	89	88	87	86	84
$\langle r_{6s}\rangle_{rel}/\langle r_{6s}\rangle_{non-rel}$	0.958	0.955	0.958	0.956	0.954	0.951	0.949	0.939	0.945	0.942	0.94	0.937	0.935	0.932	0.916
$\langle r_{4f}\rangle_{rel}/\langle r_{4f}\rangle_{non-rel}$		1.054	1.067	1.059	1.054	1.064	1.062	1.049	1.06	1.059	1.059	1.059	1.059	1.06	1.05
D_0	2.5	2.57	1.3	0.82		0.52	0.43	1.8	1.4	0.69	0.82	0.74	0.52	0.13	1.43
D_0^d	3.16	3.15	3.3	1.87		0.52	0.43	2.6	3.3	0.69	0.82	0.74	0.52	0.13	3.77
ω_e	236.0	245.4	244.9	148.0				138.7	137.6						121.6
k_e	2.28	2.48	2.49	0.93				0.89	0.88						0.76
term symbol	$^1\Sigma_g^+$	$^1\Sigma_g^+$	$^1\Sigma_g^+$	$^5\Sigma_u^-$				$^5\Sigma_u^-$	$^5\Sigma_u^-$						$^5\Sigma_u^-$

[a] Note that there are experimental indications that the dimer ground-state term symbols are either $^1\Sigma_g^+(\sigma_g^2\pi_u^4)$ or $^5\Sigma_u^-(\sigma_g^2\sigma_u^1\sigma_g^1\pi_u^2)$ or as indicated. Those not listed are most likely $^1\Sigma_g^+(\sigma_g^2\sigma_u^2)$, but there is no direct evidence for this since there are no observed spectra.

and b_{ij} is a constant determined by the rows in the periodic table of the two bonded atoms. Pauling originally estimated b_{ij} to be about 0.6 for many species. In our case we take, as above, the bond order for the coinage metal dimers ($d^{10}s^1$ atomic configuration) to be 1. In Table 3, internuclear distances are known for each of these. For dimers of the first row of the transition metals we take $b_{ij} = 1.00$ and for the second row $b_{ij} = 0.75$.[202] For the third row there are not sufficient measurements of internuclear distances to provide a useful comparison. In Table 3 we present the calculated values of the internuclear distance using Pauling's relation. The results of this calculation are in excellent agreement with the bond lengths that have been measured. Almost all values are within 0.1 Å, and the average deviation is 0.06 Å. For the remaining dimers of the first two rows, we present a predicted internuclear distance, and it can be seen that reasonable values are obtained, but confirmation of these numbers awaits accurate experimental results. In any case, it is clear that those results for which a comparison can be made provide striking confirmation of Pauling's insight as to the intimate connection between bond length and bond order.

V. Lanthanide Dimers

A. Dimer Force Constants and Dissociation Energies

Table 4 shows a comparison of several properties of lanthanide atoms and dimers including dimer dissociation energies, as measured by Knudsen effusion mass spectroscopy[203] and measured dimer force constants. Since the f orbitals are held closely to the nucleus, it is usually assumed that they do not participate in bonding. Thus, since only f electrons are being added across the lanthanides, such properties as the atomic or ionic radii vary gradually and monotonically. Originally it was expected that the force constants might either vary monotonically across the lanthanides following Badger's rule ($k_e(r_e - d_{ij})^3 = C$) or track the measured dissociation energies (see Table 4). Instead, those measured fall into two sharply distinct groups, either close to 2.28 mdyne/Å (La_2, Ce_2, and Pr_2) or close to 0.88 mdyne/Å (Nd_2, Gd_2, Tb_2, and Lu_2). It is clear that the added f electrons have at least an indirect effect on dimer bonding. This is confirmed in several cases by the calculations of Dolg, Stoll, and Preuss.[204] Following Pauling's rule that force constants are a linear function of the bond order and recognizing the similarity to Y_2 ($k_e = 0.90$ mdyne/Å), the lower group of force constants may safely be ascribed to a lower bond order of around 1 or 2 while the higher group then corresponds to a higher bond order, say between 2 and 3. This observation is suggestive of a possible shift in ground-state configuration between Pr_2 and Nd_2. In earlier work the relatively high force constant in La_2 was attributed to the very low 6s → 5d promotion energy in La (see Table 4). However, this does not adequately explain the similarly large value in Ce_2 and Pr_2. Support for the assignment of a double- or triple-bonded ground state in La_2, Ce_2, and Pr_2 can be obtained, as in section IV.B above, by calculating the diabatic bond energy D_e^d and by adding the dissociation energy to twice the (6s → 5d) promotion energy. The rather high values of 3.16, 3.15, and 3.3 eV, respectively, are obtained. This holds despite the high promotion energy for Pr. The apparently weaker (adiabatic) bond dissociation energy for Pr_2 is simply the result of the higher promotion energy needed to obtain the $6s^15d^2$ configuration. Note that the force constant measurements correctly assess this tradeoff.

It is clear that we must examine more carefully the influence of 4f electrons on bonding in the valence shell. Any discussion of the effect of f electrons on the bonding in transition metals and lanthanides must consider two contravening effects. One is due to the incomplete shielding of the 5d and 6s electrons by the f electrons, and the other is the increasing influence of relativistic effects with increasing nuclear charge. It is well understood that 4f electrons cannot effectively shield the outer electrons of the 5p, 5d, and 6s orbitals, leading to a rather higher effective charge felt by these electrons. The atomic radius of La is 107 pm while that of Lu is only 84 pm (see Table 4), almost the same as that of Y (88 pm). This orbital contraction (sometimes called the "lanthanide con-

traction") leads, among other things, to the observation of nearly equal atomic radii for the second- and third-row transition metals (e.g., Hf and Zr, Ta and Nb, etc.). If this were the only effect, we might expect a rather monotonic change in force constants across the lanthanides following the monotonic decrease in both atomic and ionic radii (see Table 4). This is obviously not the case either for force constants or dissociation energies. Clearly, relativistic effects must also be of consequence. Due to the mass−velocity term in the Dirac Hamiltonian, the 6s orbital is contracted by relativistic effects while the 4f and 5d electrons experience an expansion. These effects have been explored in great detail in a very useful article by Desclaux,[191] who has calculated orbital energies and expectation values for various powers of the radius for atoms with $Z = 1-120$. A comparison is made between relativistic Dirac−Fock calculations and those of previous nonrelativistic results. In Table 4 we present the ratio of the relativistic value of $\langle r \rangle$ to the nonrelativistic value for the 6s and 4f orbitals. For the 4f orbital these ratios are 1.054, 1.067, 1.059, and 1.036 for Ce, Pr, Nd, and Gd, respectively. Note, first, that for the 4f orbital (and presumably the 5d orbital, when occupied) the ratio is greater than one, indicating a relativistic expansion, while for the 6s orbitals the ratio is less than one, resulting in a contraction due to relativity.

Relativistic configuration-interaction calculations by Schwerdtfeger and Dolg[205] show remarkably large relativistic correction to the bond length and vibrational frequencies of AuLa and AuLu. As an example, the calculated Au−La force constant increases by over 160% due to inclusion of relativistic effects. Thus, it would not be surprising that the additional relativistic contraction to the Pr radial expectation values were responsible for the higher than expected Pr_2 force constant. It is obvious that more accurate relativistic calculations are necessary in order to unravel the various countervailing tendencies.

B. Dimer Optical Spectra and Calculations

Further insight can be gained as to the nature of the lanthanide dimers by examination of their optical spectra. We may be assisted in this regard by turning to theory. Calculations in molecules with such high atomic numbers are difficult due to increasing importance of relativistic effects.[189] Dolg, Stoll, and Preuss[204] used quasirelativistic pseudopotentials in a configuration interaction and correlation density functional study of lanthanide dimers. The 4f electrons were assumed not to have any direct involvement in bonding, so that the orbitals obtained for the low-lying states are based solely on the 6s and 5d atomic orbitals. The first σ_g and σ_u are bonding and antibonding combinations of 6s atomic orbitals, respectively, while the remaining orbitals derive from the 5d electrons, the σ_g and π_u are bonding in character, while the δ_g is only weakly bonding. Thus, we may assign a formal bond order to each of the states as shown in parentheses after each term symbol. Dolg, Stoll, and Preuss found five low-lying states containing between four and six valence electrons, a $^5\Sigma_u^-(\sigma_g^2\sigma_u^1\sigma_g^1\pi_u^2)$ (2), $^1\Sigma_g^+(\sigma_g^2\pi_u^4)$ (3), $^1\Sigma_g^+(\sigma_g^2\sigma_u^2\sigma_g^2)$ (1), $^1\Sigma_g^+(\sigma_g^2\sigma_u^2)$ (0), and a somewhat higher $^5\Delta_u(\sigma_g^2\sigma_u^1\pi_u^2\delta_g^1)$ (2). These do not represent the total term symbols but simply describe the portion of the molecule that excludes the 4f electrons. By examining the pattern of the observed force constants, we may infer that La_2, Ce_2, and Pr_2, with a force constant near 2.28 mdyne/Å, have the same ground state, whereas Nd_2, Gd_2, Tb_2, and Lu_2, with force constants near 0.88 mdyne/Å, have a different one. The $^1\Sigma_g^+(\sigma_g^2\pi_u^4)$ is a probable candidate for the first three since it has the highest formal bond order (3). Since the $^1\Sigma_g^+(\sigma_g^2\sigma_u^2\sigma_g^2)$ or the $^5\Sigma_u^-(\sigma_g^2\sigma 1\sigma\pi_{ugu}^{12})$ both have a lower formal bond order, this suggests either one of them for the ground state of the remaining four dimers. However, the observation of an extremely large magnetic moment in Gd_2 indicates a $^{19}\Sigma_g^+$ ground state.[206] This conclusion is confirmed by a recent fully relativistic density functional calculation by Dolg, Liu, and Kalvoda[207] that allows spin realignment in the $4f^7$ cores. Assuming strong ferromagnetic coupling of the two sets of $4f^7$ electrons, this high-spin state most likely originates from the $^5\Sigma_u^-(\sigma_g^2\sigma_u^1\sigma_g^1\pi_u^2)$ state. It is thus reasonable that the four dimers with the lower force constant also have this ground state. Confirmation of this assignment comes from the fact that the ground state of Sc_2 and Y_2 (with force constants of 0.76 and 0.89 mdyne/Å) has been established by ESR spectroscopy. The remaining dimers, for which Raman spectra could not be obtained (Pm_2, Sm_2, Eu_2, Dy_2, Ho_2, Er_2, Tm_2, Yb_2), all have 6s → 5d promotion energies greater that 1.34 eV, making it likely that the ground state of these molecules derives from two $4f^n6s^2$ atoms. This, combined with observation of very low dissociation energies, indicates that they have the nonbonding $^1\Sigma_g^+(\sigma_g^2\sigma_u^2)$ for a ground state.

In terms of dissociation, those dimers which have a $^1\Sigma_g^+(\sigma_g^2\pi_u^4)$ ground state (i.e., La_2, Ce_2 and Pr_2) correlate with two $4f^n6s^15d^2$ ($n = 0, 1, 2$) states in the separated atom limit while those which have a probable $^5\Sigma_u^-(\sigma_g^2\sigma_u^1\sigma_g^1\pi_u^2)$ ground state (i.e., Nd_2, Gd_2, Tb_2, and Lu_2) correspond to $4f^n6s^15d^2 + 4f^n6s^25d^1$ ($n = 3, 7, 8, 14$) separated atoms. The remaining dimers with the likely nonbonding ground state $^1\Sigma_g^+(\sigma_g^2\sigma_u^2)$ probably dissociate to two $4f^n6s^2$ atoms, and no promotion energy is needed to determine the diabatic dissociation energy of these dimers, which is quite small in any case.

In Table 5 we collect the results from either absorption, SDS, or Raman excitation profiles of numerous lanthanide dimers. [These absorption bands are taken from refs 42 (Y_2), 45 (La_2), 27 (Ce_2, Pr_2, Nd_2), 208 (Sm_2), 28 (Gd_2), 46 (Tb_2), 209 (Dy_2), 210 (Ho_2), 211 (Yb_2), 47 (Lu_2), and 57 (Hf_2).] Included for comparison are the bands in Y_2 and Hf_2 as well. Note that all observed dimer spectra show one or more of three distinct bands, centered at approximately an average of 485 (blue), 549 (green), and 631 nm (red). Even though not all three bands appear for each dimer, the constancy of the observed wavelength

Table 5. Lanthanide Dimer Optical Transitions (nm)

	blue	green	red	ref
Y_2	485			42
La_2	490	540,560		45
Ce_2	485	547		27
Pr_2	465	535		27
Nd_2		520	640	27
Sm_2		541	599	208
Gd_2		585	620	28
Tb_2			633,645	46
Dy_2		520	575	209
Ho_2	498,504	558,562		210
Yb_2		555		211
Lu_2	505	540	640,652	47
Hf_2	450	540	620	57

across the series is remarkable. Still, more remarkable is that the energy spacing of these average bands (i.e., blue-green and green-red) is the same, around 2380 cm^{-1}. It is, of course, possible that these numbers are coincidental. More likely they reveal an underlying set of electronic states, which are common to all lanthanide dimers. The intensity of these bands indicates that they correspond to an allowed atomic transition, say a nearby allowed 6s → 6p transition. In atomic lutetium the $^4F^o$ ($4f^{14}5d6s6p$) state could lead to an excited $^3\Pi$, giving an equally spaced triplet with $\Omega = 0, 1, 2$. The atomic 6p spin−orbit coupling constant may be inferred from atomic energy levels[212] to be $\zeta(6p) = 3454$ cm^{-1}. To the extent that the spin−orbit splitting of the excited state is first order,[213] we predict $A = 1/2(3454) = 1727$ cm^{-1}, somewhat lower than the observed value of 2380 cm^{-1} but certainly of reasonable magnitude. Of course, too much should not be read into the lack of observation of a transition, especially for those as broad as observed here. However, it is provocative that for La_2, Ce_2, and Pr_2 the blue and green transitions are observed, while for the remaining dimers, starting at Nd_2 (except Ho_2 and Lu_2), it is the green and red transitions which appear. This is the same place (i.e., between Pr_2 and Nd_2) that a break is observed in the force constants, indicating a sharp change in the orbital nature of the ground state. Despite considerable disparities in properties across the lanthanides, we observe remarkable consistency in spectroscopic properties. The observed force constants fall into two narrow categories, while the three observed visible transitions are nearly invariant in wavelength, although their intensity distributions appear to fall into the same two categories.

C. Periodic Properties

The observed frequency for La_2 leads to a force constant of $k_e = 2.28(1)$ mdyne/Å. The corresponding values for Sc_2 and Y_2 are 0.756 and 0.90 mdyne/Å, respectively. This trend is in marked contrast to the adjacent column: Ti_2 (2.35 mdyne/Å), Zr_2 (2.511 mdyne/Å), and Hf_2 (1.63 mdyne/Å). The same anomaly is apparent if we compare force constants along the same row. In the first and second row of transition-metal dimers, the group 3 force constants are lower than those of the adjacent group 4, 5, and 6 force constants. For La_2, in the third row, the force constant is higher than that of Hf_2. This analysis

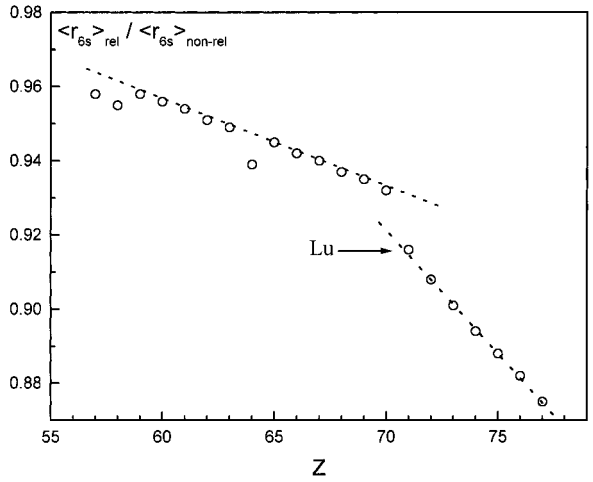

Figure 4. Ratio of relativistic to nonrelativistic 6s orbital radial expectation value for atoms with $Z = 57-77$. The value for Lu fits more closely with those of higher Z than with the other lanthanides. The deviations of La (57), Ce (58), and Gd (64) are due to the fact that these elements have a single 5d electron in their ground configuration while the remaining lanthanides have an empty 5d subshell.

raises the question as to whether it would be more suitable to replace La with Lu in the periodic table. The lower value for the Lu_2 force constant measured here fits the trends for the other rows and columns better than that from La_2. In fact, this replacement has been suggested by several other observers. For example, Jensen[214] analyzed just this issue. He shows various trends in atomic radii, ionization potentials, melting points, and electronegativities which support his contention. This idea is further supported by the above assignment of the ground state of Lu_2 as $^5\Sigma_u^-$-($\sigma_g^2\sigma_u^1\sigma_g^1\pi_u^2$), which is the same as that for Sc_2 and Y_2, while La_2 most likely has a different ground state (see Table 2). In addition, examining the calculations of Desclaux[191] of the ratio of relativistic to nonrelativistic 6s orbital radial expectation values (see Figure 4), it can be seen that across the lanthanides there is a steady but gradual decline until Lu, where the ratio abruptly drops to a value nearer that of Hf. For these reasons, in all our tables of transition metals, listing periodic properties, we use Lu where La usually resides.

V. Trimers

For trimers, it is often the case that insufficient data is obtained for a complete normal coordinate analysis.[74,128] The symmetric stretch ω_a is usually obtained, but the degenerate bend ω_e (for the equilateral triangle in D_{3h}) or the split asymmetric stretch and bending modes (for the bent C_{2v}) are either not obtained or of sufficiently dubious assignment to be of much use for reliable force field determination. However, most of the observed trimers are either equilateral triangles or close, and in the central force approximation, the bond stretching force constant is related to the breathing mode frequency ω_a. This may be obtained by utilizing the formulas from Herzberg[74] for central force trimer frequencies with atomic

Table 6. Ground-State Trimer Force Constants (mdyne/Å) for Transition Metals[a]

Sc_3	Ti_3	V_3	Cr_3	Mn_3	Fe_3	Co_3	Ni_3	Cu_3	Zn_3
0.54		2.21	1.91	0.37	0.68		0.62	.91/.66	
Y_3	Zr_3	Nb_3	Mo_3	Tc_3	Ru_3	Rh_3	Pd_3	Ag_3	Cd_3
	1.19	2.05	2.82		1.86	2.10		0.55	
Lu_3	Hf_3	Ta_3	W_3	Re_3	Os_3	Ir_3	Pt_3	Au_3	Hg_3
	0.72	2.25					1.93	1.25	

[a] Metals in red were studied in mass-selected experiments.

masses and force constants set equal. The result is

$$\lambda_1 = \omega_1^2 = 3\,(k_e/m)$$

$$\lambda_2 = \omega_2^2 = 2\cos^2(\phi/2)(k_e/m)$$

$$\lambda_3 = \omega_3^2 = (3 - 2\cos^2(\phi/2))(k_e/m)$$

In the equilateral triangle limit with the angle $\phi = 60°$, we obtain the bond stretching force constant $k_e = m\omega_a^2/3$ (using the same conversion factor as above, i.e., 1 amu $cm^{-2} = 5.8919 \times 10^{-7}$ mdyne/Å) and $\omega_a = \omega_1$ while $\omega_e = \omega_2 = \omega_3$. It can easily be seen that $\omega_a/\omega_e = \sqrt{2}$. For slight deviations from an equilateral triangle, the degenerate vibrations will be split slightly, and that splitting may be used to obtain an approximate, though crude, value for the angle ϕ.

By way of comparison, sufficient data was available for a more sophisticated normal mode calculation in Mn_3,[91] and the authors obtained a stretching force constant of 0.38 mdyne/Å with a stretch−stretch interaction constant of 0.02 mdyne/Å. Using the central force approximation we obtain a value of 0.42 mdyne/Å.

In Table 6 we list the trimer force constants obtained by choosing the best force constants, either with normal mode calculations or, where the data is insufficient, with the simple central force approximation. This table is not as complete as that for the dimers, since somewhat less extensive research has been carried out on the trimers. However, to the extent that the data exists, it can be seen that it mostly follows the trends observed in the dimer table. Early in each period there is a sharp increase in force constant, reflecting the increasing number of d electrons which may participate in bonding, while late in each period we observe a decline in the force constant due to decreasing size of the d orbitals and increasing occupation of antibonding orbitals in the metal dimers. The center of the first row shows a sharp decline in the magnitude of the force constant near Mn, reflecting the high stability of the $3d^54s^2$ configuration of atomic Mn, which makes it difficult to promote the atom to a state which can support strong bonding. This is discussed in more detail below. In the center of the second row, the force constants remain high, in a manner similar to the dimer pattern, presumably for similar reasons. The third row presents too little data near the center for any analysis.

Any detailed comparison of dimer and trimer force constants should take into account the work of Ozin and McIntosh.[215] In considering the force constants of various silver clusters, they proposed a scheme to predict the force constants of higher clusters from that of the dimer. They suggest a bond-connectivity force field in which the bond stretching force constants are determined by taking account of the number of metal−metal bonds to nearest neighbors. This involves simply calculating (α_n) the sum of the number of atoms to which each atom in a bond is connected. Then the factor $\beta_n = 2/(\alpha_n)$ is multiplied by the dimer force constant.

$$k^{(n)} = \beta_n k^{(2)}$$

For example, in an equilateral triangle this factor is $\beta_3 = 1/2$, while for a linear trimer it is 2/3. For C_{2v} symmetry, we might expect a ratio somewhere between 1/2 and 2/3. For a tetrahedral tetramer (T_d) the factor is $\beta_4 = 1/3$, while for a rhomboidal tetramer (D_{2h}) the factor is $\beta_4 = 2/5$ for the peripheral bonds and 1/3 for the diagonal bond. For many of the observed higher cluster force constants, this has been found to be a reliable guide. We shall explore this in more detail both in a later section and in Appendix B, where the rules are applied to small clusters of the alkali metals, alkaline earth metals, as well as P and As. However, it is worth noting the relationship of this approach with Pauling's rule. If the force constant is indeed a direct measure of the bond order, then the procedure recommended by Ozin and McIntosh amounts to assuming that in forming a larger cluster from a smaller one, the bond order (or perhaps electron density) is spread out evenly among the adjacent new bonds. Some of these ideas were anticipated in generalized valence bond calculations of McAdon and Goddard,[216] in which bonding in metallic clusters could best be described in terms of interstitial orbitals localized at the centers of equilateral triangles for planar structures and in the centers of tetrahedra for three-dimensional clusters.

Of course, an underlying assumption of Ozin and McIntosh is that there is no change in type of bonding or configuration from one cluster to a larger one. For example, a dimer might be held together by van der Waals bonding while the trimer or some higher cluster might experience the onset of covalent bond-

Table 7. Ratio of Trimer Symmetric Stretch Force Constant to the Dimer Force Constant for Transition-Metal Clusters

Sc	Ti	V	Cr	Mn	Fe	Co	Ni	Cu	Zn
0.71		0.51	0.54	4	0.46		0.53	.68/.50	
Y	Zr	Nb	Mo	Tc	Ru	Rh	Pd	Ag	Cd
	0.47	0.42	0.44		0.52	0.86		0.47	
Lu	Hf	Ta	W	Re	Os	Ir	Pt	Au	Hg
	0.44	0.47					0.68	0.59	

ing. Also conceivable would be the possible lowering of some excited configuration of, say, a dimer due to interactions with an approaching atom or cluster, resulting in a change in the configuration of the newly formed larger cluster. In fact, deviations from these predictions might be considered a good test of whether bonding type remains constant with increasing cluster size.

Let us examine, where possible, the ratio of trimer stretching force constant to dimer force constant. These results are shown in Table 7. Those trimers that have D_{3h} symmetry should display a factor of 0.5, and it can be seen that most of the observed values are close to that number. The most telling exception is that of Mn_3, which shows a ratio near 4. Since the dimer is a van der Waals molecule and the trimer is most likely bound covalently, this is the type of situation expected to produce a deviation from the Ozin and McIntosh rules. A similar effect has been observed in a study of the clusters of Mg.[217] The force constant observed in Mg_2 is 0.071 mdyne/Å, while that for Mg_4 is 0.15 mdyne/Å. Since the atomic configuration of Mg has a filled $3s^2$ orbital, the low force constant in the dimer is attributed to a van der Waals bond, while the much larger force constant in the tetramer has been interpreted by Kornath as indicative of the onset of covalent bonding. Other smaller deviations include Sc, Rh, Pt, and one of the two possible values for Cu. In these cases the deviation is most likely either due to deviations in the geometry (C_{2v}) from an equilateral triangle or may be an indicator that the trimer bond is formed, for example, from a different orbital configuration than that of the ground state of the dimer.

Note that most of the other trimers have a ratio of trimer to dimer force constant near enough to 0.5 to fit well the expectations of Ozin and McIntosh, indicating little or no serious change in bonding of formation of the trimer. The trimers exhibit a wide range of force constant magnitudes. In the first row V_3 and Cr_3 have rather large stretching force constants compared to the other members of the first row. This indicates that the relatively strong bonding observed in the dimers persists in the trimers. In the second row Mo_3 also displays a rather high force constant, in fact the highest yet observed for a transition-metal trimer (2.80 mdyne/Å). The very high dimer bond order (see Figure 2), which is likely due to the availability of a large number of d electrons for bonding, undoubtedly shows considerable influence on the trimer bonding as well. As with the dimers, it can be observed that the force constants in the late third row for Pt_3 and Au_3 are considerably higher than those above them in the table. This is in contrast to both the dimers and trimers earlier in this row and probably reflects the especially large relativistic effects in Pt and Au, which cause the 6s orbital radius to contract while the 5d radius expands, leading to shorter bond lengths and concomitant higher force constants.

Table 8. Experimental Force Constants for Larger Transition-Metal Clusters[a]

cluster size	Ag	Au	Ta	Nb
2	1.18	2.115	4.80	4.84
3	0.556/0.285(0.59)	1.25(1.06)	2.25(2.40)	1.95(2.42)
4			1.89(1.60)	
5	0.5(0.47)			
6		0.226(0.423)		
7	0.259(0.26)			
8				(0.99−1.24)
9	0.195(0.182)			
∞ (13)	0.09(0.098)	0.217(0.176)		

[a] Values in parentheses are those predicted by the scheme of Ozin and McIntosh (Ozin, G. A.; McIntosh, D. F. *J. Phys. Chem.* **1986**, *90*, 5756) using the force constant of the dimer. For the crystal (face-centered cubic) we take $n = 13$, corresponding to a coordination number of 12.

VII. Higher Clusters

A. Transition Metals

One of the goals of cluster science is to determine the relationship of various parameters as a function of cluster size with the idea of understanding at what point bulk properties become manifest. The previous discussion has been concerned with force constants of dimers and trimers, since a good deal of the reliable spectroscopy to date has been carried out on these species. However, some spectra exist for higher clusters of several species, and force constants have been deduced from these measurements. As clusters become larger, the force field becomes more complex, with more possible combinations of force constants, yet often only a few of the possible distinct frequencies may be observed in an experiment. Thus, it becomes more difficult to extract a unique set of force constants from the vibrational frequencies, and we must necessarily make some approximations to arrive at a reasonable analysis.

Tantalum is the only transition-metal cluster for which force constants exist for dimer, trimer, and tetramer.[71−73] We present a comparison of the Ta−Ta stretching force constants obtained for each of these clusters in Table 8. According to the previously mentioned scheme of Ozin and McIntosh,[215] for an equilateral triangle (D_{3h}) trimer the force constant should be 1/2 that of the dimer, while for a linear trimer the factor is $\beta_2 = 2/3$, and for a tetrahedral (T_d) tetramer the factor should be $\beta_3 = 1/3$. The predicted values are presented in parentheses in the table. As can be seen, the predictions are quite close to the measured values. For the trimer, the difference may be due to deviations of the geometry from that of an equilateral triangle. We might expect a C_{2v} trimer to have force constants intermediate between

those expected for the equilateral triangle and those of the linear molecule. Since lower frequency modes were not observed, structural information about this trimer is not available.

For silver, thanks to the work of Moskovits and coworkers,[105] we have the most complete picture for any metal. For the trimer, there are two possible force constants due to the disagreement between several differing experimental techniques. For completeness we include both possibilities. Only the larger value is close to the predicted value. While this is no particular reason to reject the smaller value, if this lower figure is in fact the correct value, it implies a drastic change in the type of bonding for the trimer compared with the other silver clusters (both the dimer and higher clusters). In the pentamer, Moskovits et al.[175] were able to fit the observed spectrum adequately using a bond stretching force constant of 0.5 mdyne/Å for a planar trapezoid. Applying the rules of Ozin and McIntosh to such a structure produces a factor of $\beta_5 = 2/5$, resulting in close agreement with the experimental value.

To examine the heptamer and nonamer[161] in this fashion, we must make a few assumptions. The experimentally observed frequencies are most likely the totally symmetric breathing modes, since these would be expected to give the highest Raman intensity. Assuming that all the atoms are bound to each other with an equal force constant and reasoning by analogy with formulas for the force constants obtained from the totally symmetric vibration in dimers, trimers, and tetramers (see above) we may obtain a crude approximation to this value by taking $k^{(n)} = m\omega^2/n$, where m is the atomic mass, ω is the observed frequency, and n is the number of atoms in the cluster. Under the same assumption, the Ozin and McIntosh factors for the heptamer and nonamer would be $\beta_7 = 2/9$ and $\beta_9 = 2/13$, respectively. We can take this a step further by examining the crystalline silver. The force constant for a crystal may be obtained by fitting phonon dispersion measurements with an assumed force field in a manner similar to a normal coordinate analysis of observed frequencies for a molecule. Only nearest-neighbor interactions are needed. The experimentally observed radial force constant for silver[218] is 0.09 mdyne/Å. For a face-centered cubic crystal the coordination number for nearest neighbors is 12, and applying the rules of Ozin and McIntosh to this structure, we obtain a factor of $\beta_{13} = 1/12$, resulting in a predicted force constant of 0.098 mdyne/Å. These values are in remarkable agreement. A similar analysis for face-centered cubic Au gives 0.176 mdyne/Å, compared with the experimental result of 0.217 mdyne/Å.

In Figure 5 we plot the experimental and predicted force constants ($k^{(n)}$) of various silver clusters against the cluster size n. For comparison we plot the curve of $k^{(n)}$ against $k^{(2)}/(n-1)$. This is what we might expect using a Jellium-like model, in which all the nuclei are treated equally and that the electron density is distributed uniformly among the atoms, resulting in a set of equal stretching force constants. Recognizing that the maximum number of atoms to which a given atom may be bonded is $n-1$, it is clear

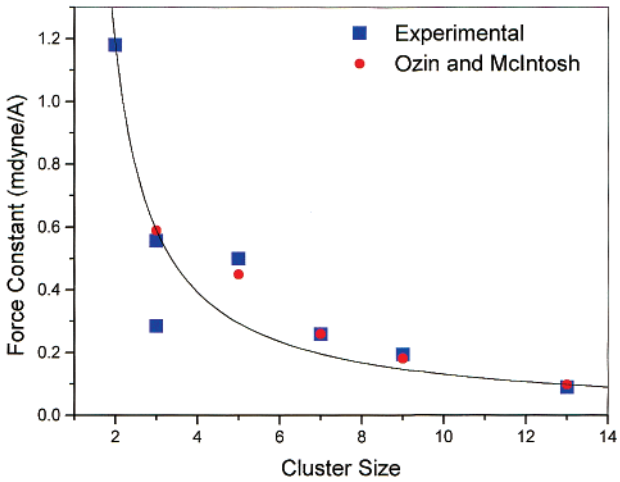

Figure 5. Size dependence of experimental values for the bond-stretching force constants in silver clusters (Ag_n). Squares represent measured values taken from spectra. The face-centered cubic crystal structure is shown as $n = 13$, since the coordination number for nearest neighbors is 12. Circles represent values predicted (from the dimer) using the scheme of Ozin and McIntosh.[215] Note two possible experimental values are given for the trimer, reflecting conflicting experimental results. The solid curve represents a calculation assuming the force constant (scaled from the dimer value) varies simply as the inverse of the coordination number ($n-1$).

that for this Jellium-like model the rules of Ozin and McIntosh would lead to $\beta_n = 2/[(n-1)+(n-1)] = 1/(n-1)$. This therefore represents a lower limit on the Ozin and McIntosh force constants. The curve in Figure 5 shows that this can be seen to provide a reasonable, if crude, depiction of the variation of force constant with cluster size in silver clusters, with the planar pentamer providing the greatest deviation. Notice the Jellium-like model predicts the crystal force constant exactly, and the heptamer and nonamer values are likewise quite close.

The predictions of Ozin and McIntosh, which take into consideration details of geometry, approximate the experimental results much better than the Jellium-like model (except for one of the possible trimer values). This provides a justification for the interpretation of their rules as simply a redistribution of bond order as cluster size increases. A numerical justification for such an approach has recently been provided by the density functional calculations of Kua and Goddard[142] on platinum clusters, in which it was found that the calculated cohesive energies of Pt_n clusters could be written $E_{coh} = (n-1)85$ kcal/mol. This was interpreted as indicating that each additional atom added to a cluster results in a constant contribution to the cohesive energy.

Using vibrational autodetachment spectroscopy of mass-selected Au_6^-, Taylor et al.[219] observed a single vibrational progression of Au_6, which is at 108 cm^{-1}. They recommend a hexagonal ring structure (D_{6h}) and predict a symmetrical ring breathing (a_g) normal mode for this vibration. Applying the model used above for silver ($k^{(n)} = m\omega^2/n$), we obtain a force constant of 0.226 mdyne/Å. Comparing with the Ozin and McIntosh model, we obtain a predicted force constant of 0.423 mdyne/Å. As shown above, a similar disagreement is found for the crystal force constant

in gold. Note, for all the gold clusters greater than the dimer, there is a rather large discrepancy between the observed value of the force constant and that predicted by the Ozin and McIntosh model. This is in considerable contrast to the much better characterized silver clusters and possibly reflects changes in the type of bonding between the dimer and higher clusters, or perhaps large geometric deviations from the presumed structures, or a failure of the Ozin−McIntosh model.

The other larger cluster for which vibrational data exists is Nb_8. In a mass-selected negative-ion photoelectron study, Marcy and Leopold[220] found a clear vibrational progression of 180(15) cm^{-1}. They assumed a C_{2v} bicapped octahedral structure, as predicted by several DFT studies. This structure has seven totally symmetric a_1 vibrational normal modes. They used the rules of Ozin and McIntosh to derive a force field giving values ranging from 0.99 to 1.24 mdyne/Å for various bonds. These assumptions resulted in reasonable values for the predicted vibrational frequencies (150−200 cm^{-1}). With only one observed progression, however, it is difficult to decide among other reasonable alternatives.

This approach is still very rudimentary, and new experimental techniques will be needed to obtain accurate structural and vibrational data on larger clusters. However, the appeal of this approach is that it can provide considerable insight into the connection between the properties of small clusters and bulk metals.

The TOF−PES experiments of Wang and co-workers[30] have shown that with respect to properties such as electron affinities, ionization potentials, and chemical reactivity, clusters of Fe exhibit bulklike behavior around Fe_{25}, similar to that observed in Cr[221], while for Ti[222] and V[223] the onset of bulk behavior occurs at much lower cluster size (Ti_{10} and V_{17}).

B. Higher Lanthanide Clusters

Relatively little work has been carried out on larger clusters of lanthanides. Klotzbucher and co-workers[224] assigned absorption bands of Ho_3 at 608 nm and Ho_4 at 450 nm. Ionization potentials of Ce_n (n = 2−21) and Pr_n (n = 2−17) clusters have been measured.[225] The potentials vary discontinuously with cluster size, clearly indicating structural discontinuities. These observations were also taken as evidence for the $4f^36s^2 \rightarrow 4f^2(5d,6s)^3$ transition, which appears at n = 5. A smaller step is observed at n = 13−15. Similar discontinuities in atomic volume as a function of grain size were observed for clusters of Yb and Eu.[226] The sharp discontinuity at around grain size 300 $Å^{-1}$ results in a sudden drop of 27% in atomic volume. This was also taken to suggest a change in the fcc bulk metal to the normal rare earth $4f^{n-1}(5d, 6s)^3$ configuration.

The magnetic properties of Gd clusters have been the subject of several studies. Douglass, Bucher, and Bloomfield[227] found magic numbers for Gd_n (n = 11−92) in the mass spectra of magnetically deflected species. At n = 22, 30, and 33, very large superparamagnetic moments are observed. For example Gd_{22} exhibits a magnetic moment of 3.15(30) μ_B per atom.

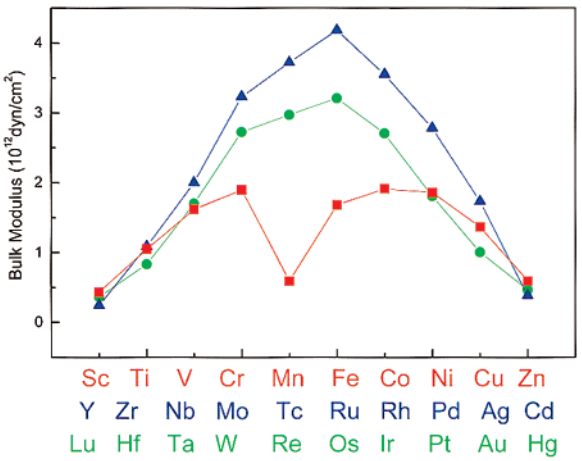

Figure 6. Bulk moduli for transition metals. Squares are for the first row, triangles for the second row, and circles for the third row.

A later study in a Stern−Gerlach magnetic deflection beam[228] found that Gd_{22} clusters show deviations from linear behavior expected for superparamagnetic moments with vibrational temperature. Bucher and Bloomfield[229] conclude that there is a strong difference between the response of transition-metal (3d) and lanthanide (4f) ferromagnets due to a significant difference in the importance of magnetic anisotropy and exchange energy.

VIII. Bulk Properties

One of the goals of cluster science is to determine the relationship of various parameters in small clusters with the idea of understanding to what extent analogous bulk properties may be predicted. The bulk modulus, the reciprocal of the isothermal compressibility, provides a good candidate for such an examination. It is defined as

$$B = -V\frac{dp}{dV}$$

where V is the volume and p is the pressure. Using the thermodynamic identity for the energy $dU = -p\,dV$ then $dp/dV = -d^2U/dV^2$ and we have

$$B = V\frac{d^2U}{dV^2}$$

This is a good measure of the compressibility of the crystal. In this case U may be considered to represent the cohesive energy of the crystal and $U(V)$ plays the same role as the nuclear potential energy does for dimers or small clusters. In fact, plots of U versus V[230] look remarkably similar to potential energy curves for diatomic molecules. The bulk modulus, as defined above, is the bulk phase analogue of the force constant, defined previously as the second derivative of the diatomic potential curve at equilibrium. We might, then, expect a close relationship between the variation of the bulk moduli[231] and the dimer force constants across the periodic table. This is illustrated in Figure 6, in which we have plotted the experimental bulk moduli for the transition metals. Comparing it with Figure 2 we see almost exact parallels for each

row of the periodic table, and thus, the diatomic force constant may be considered the diatomic precursor to metallic cohesion. Clearly the relative contributions of d electrons to bonding and even considerations of the effects of s → d promotion energies which explain the observed dimer force constants are preserved in the bulk.

This idea is made explicit in determination of the crystal binding energy of inert gas crystals, which (neglecting kinetic energy factors) may be obtained by summing the dimer Lennard−Jones potential over all pairs of atoms in the crystal (Kittel,[231] p 82). Making small quantum corrections for kinetic effects produces remarkably accurate values for the lattice parameters.

The application of these methods to transition metals has been pioneered by Pettifor.[202] The conduction band in transition metals involves a tightly bound valence d band, which overlaps and hybridizes with a broader nearly free-electron sp hybrid contribution. The tight binding approximation[232,233] allows the assumption of a rectangular-shaped density of states for the d electrons, which may be written

$$n_{\mathrm{d}}(E) = \frac{10}{W}$$

The factor of 10 is the maximum number of electrons in the d orbital, and W is the constant bandwidth. The d bond energy may then be obtained[234]

$$U_{\mathrm{bond}} = -\frac{1}{20} W N_{\mathrm{d}}(10 - N_{\mathrm{d}})$$

Contributions from the overlapping sp electrons are found to be constant across a series, and therefore, for our purposes, it is not necessary to account for them explicitly. Note that the d bond energy is proportional to the d bandwidth W and a factor N_{d}-$(10 - N_{\mathrm{d}})$, which is just the number of d electrons (N_{d}) available for bonding (assuming a $\mathrm{d}^N\mathrm{s}^1$ configuration) times the number of d holes ($10 - N_{\mathrm{d}}$). The cohesive energy may then be calculated by assuming a potential of the form

$$U = a N_{\mathrm{d}}{}^2 e^{-2\kappa R} - b N_{\mathrm{d}} e^{-\kappa R}$$

where a, b, and κ are constants across each row of the periodic table. Note this may be regarded as a modified Morse potential. By deriving the second moment of the local density of states, Pettifor[235] then shows that

$$W = (3b^2/5a) N_{\mathrm{d}}(10 - N_{\mathrm{d}})$$

and derives an expression for the bulk modulus which may be written as

$$B = \frac{\sqrt{2} b^2 \kappa^2}{300 a R_0} [N_{\mathrm{d}}(10 - N_{\mathrm{d}})]^2$$

Here R_0 is the Wigner−Seitz radius. Only a relatively slight variation of this radius is observed across the periodic table. Recognizing that for the above potential $U(R)$ we may derive a standard force constant (which is independent of the d-electron contribution and, therefore, may be regarded as a single-bond s-electron force constant), for each row in the periodic table by

$$k = \left[\frac{\partial^2 U}{\partial R^2}\right]_{R=R_0} = \frac{b^2 \kappa^2}{2a}$$

Comparing this with the bulk modulus formula, we deduce that the contributions of the d electrons will result in a variation of the force constant across the periodic table as

$$k_e = k[N_{\mathrm{d}}(10 - N_{\mathrm{d}})]^2$$

Here we have factored the force constant k_{e} into a part which is constant across the period k multiplied by a d-electron contribution, which varies across the period. Thus, the predicted d-electron contribution is just proportional to the squared factor in brackets. This rather simple model fits quite well for the third transition row, as shown in Figure 7, where we have plotted the experimental dimer force constants against N_{d} and a scaled value of $[N_{\mathrm{d}}(10 - N_{\mathrm{d}})]^2$. The corresponding (not shown) fit for the first row (3d) is marred by the drop in force constant near the center due to the especially stable d^5 configurations of Cr and Mn. The second row (4d) is fit much better but not quite as well as that for the third (5d) row.

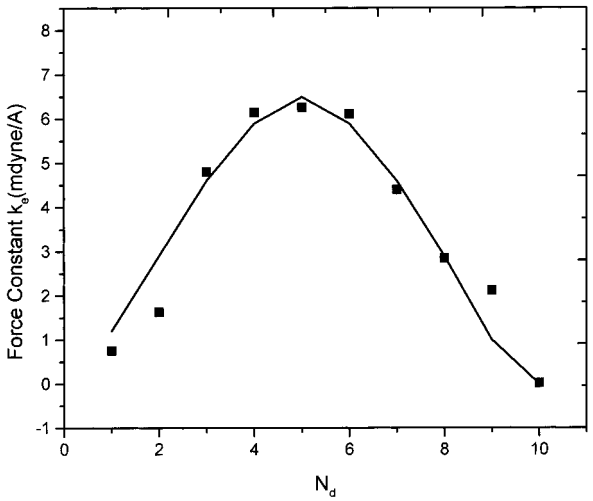

Figure 7. Third-row transition-metal dimer force constants compared with a scaled plot of $\{N_{\mathrm{d}}(10 - N_{\mathrm{d}})\}^2$, where N_{d} is the number of atomic d electrons for a $\mathrm{d}^N\mathrm{s}^1$ configuration.

In any case this illustrates the intimate connection between the dimer force constant and the bulk modulus. The overall envelope of both parameters is determined by a simple factor involving the square of the product of the number of d electrons available for bonding with the number of holes in the d shell. The increase in force constant and thus bond order early in each period is proportional to the square of the number of d electrons available for bonding $(N_{\mathrm{d}})^2$, while the decrease in force constant and bond order late in each period is proportional to the square of the number of d holes in the system $(10 - N_{\mathrm{d}})^2$. Near

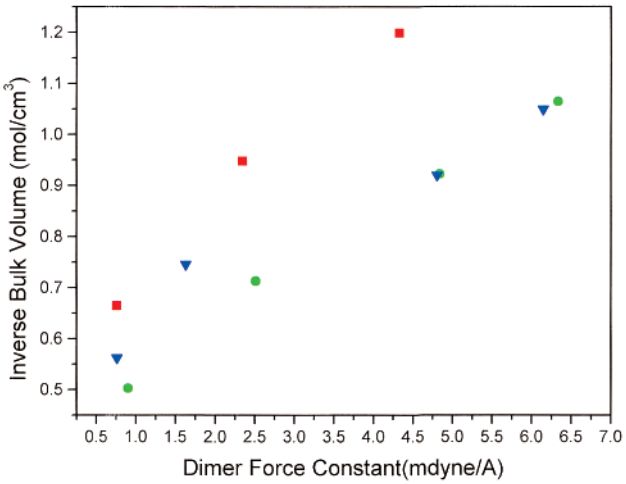

Figure 8. Inverse molar volume (mol/cm^3) plotted against the dimer force constant (mdyne/Å) for the first half of each transition-metal row. The squares, circles, and triangles represent the first, second, and third row, respectively.

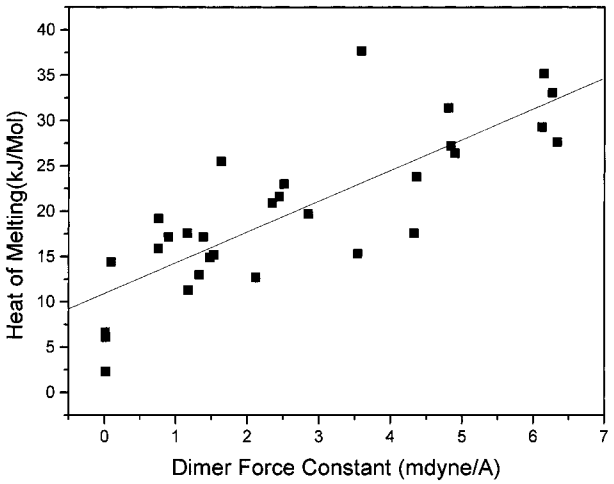

Figure 9. Heat of melting (kJ/mol) plotted against the dimer force constant (mdyne/Å) for transition metals.

the center of each period, this quadratic relationship must compete with the favorable exchange energy of the d^5 configuration in the first period as well as lesser spatial extension of the d-electron radius. In the second and third periods, however, these effects are not so severe, and a remarkably good fit to force constant and bond order variation across the periodic table can be obtained by this simple formula.

Furthermore, Pettifor[235] derived an expression for the Wigner−Seitz radius, which may be written

$$R_0 = R_1 - \kappa^{-1} \ln[N_d(10 - N_d)]^2$$

If we assume, using Pauling's rule, that the bond order is proportional to the force constant (see Figure 2) and force constants are proportional to $[N_d(10 - N_d)]^2$, we then obtain a justification for the empirical relation identified by Pauling, which we used in the previous section (section IV.E) on internuclear distances (see Table 3).

It is worthwhile examining correlations with several other bulk properties. For example, if we plot the inverse of the bulk atomic volume[236] against the dimer force constant (Figure 8), we find that for each of the periods a nearly linear relationship holds for the early transition (first half) series while for the later series metals the atomic volume varies only slightly despite larger variations in force constant. The strong linear plot is clearly anticipated by our success applying Pauling's relationship between internuclear distance and bond order (see Table 3), while the slower variation in atomic volume for late transition metals may be due to the lesser availability of d electrons for bonding, especially for the 3d series. As noted previously, the ratio of the expectation value of the orbital radii $<r_{(n)d}>/<r_{(n+1)s}>$ is found to decrease across a particular transition-metal row, and decreasing participation of d electrons in bonding is likely to result in only slight changes in both internuclear distances and atomic volumes late in each period. This effect is readily apparent in the first-row force constants (Table 1) and internuclear distances (Table 3), which change only relatively slightly for Fe through Cu.

The heat of melting for a metal also represents a bulk property, which is a measure of the strength of metallic bonding. Increasing participation of d electrons in cohesion would be expected to become manifest in the amount of heat needed to loosen those bonds during the fusion process. In Figure 9 we plot metallic heats of melting[236] (kJ/mol) against dimer force constant. A strong correlation is clear from this plot, once again revealing the degree to which dimer bonding may be considered as precursor to bulk properties, in this case an easily measurable thermodynamic property. This correlation recalls a previous fit of heats of vaporization against dimer dissociation energies by Miedema and Gingerich.[196] The authors found that they had to exclude from their fit metals for which van der Waals bonding (Mg, Zn, Cd, Hg) is present or metals which possess especially stable free atoms (Fe, Ti, V, Cr, Mn, Co, Pd). Our use of force constants rather than dissociation energies more correctly accounts for these deviations, illustrating the way in which force constants may provide a more generally applicable measure of the various contributions to chemical bonding in metals.

IX. Conclusions

We have collected and examined a large number of experimental parameters, which characterize small transition-metal and lanthanide clusters. Special attention has been paid to periodic properties of force constants, dissociation energies, and internuclear distances, and we have examined correlations of these properties to determine the degree to which d electrons contribute to metallic bonding. We have also examined the degree to which the properties of small clusters, such as dimers, can be transferred to larger species, including bulk crystalline materials. Both of these dimensions may be thought of as a challenge to theory. Although considerable theoreti-

cal advances have been made in recent years, most of the benefit has been to organic or inorganic molecules involving the lighter elements. Transition metals and lanthanides present special problems due to the contribution of d electrons, which produce large numbers of possible low-lying states. In addition, effects of correlation and relativistic effects provide daunting obstacles to accurate wave function calculations. Several recent theoretical efforts have shown promise in this regard. Yanagisawa, Tsuneda, and Hirao[237] used density functional methods to examine internuclear distances, dissociation energies, and harmonic vibrational frequencies of second- and third-row transition-metal dimers using the unrestricted Kohn−Sham technique. Their results, while still not accurate, show a great improvement over previous calculations. Tsuchiya, Abe, Nakajima, and Hirao[238] replace the effective core potential with a more accurate third-order Douglas−Kroll approximation to scalar relativistic effects. Their results on the vibrational frequencies and internuclear distances for Cu_2, Ag_2, and Au_2 are remarkably close to the experimental results.

Despite the difficulties involved in calculations, it is clear that we now have assembled a large body of accurate experimental data with which to assess theory. One challenge would be to explain, preferably with a single theoretical approach, the variation of dimer and trimer force constants (or dissociation energies) throughout the periodic table. To what extent do such empirical correlations such as Badger's rule, Pauling's rule, Pettifor's fits, etc., have underlying theoretical validity? In considering extensions of dimer properties to larger clusters, is it possible to justify the rules of Ozin and McIntosh? Under what conditions might we explain the exceptions to these rules? How can we predict more reliably the properties of larger clusters from those of dimers and trimers? Clearly more experimental work needs also be done, and of course, the interplay between theory and experiment has been and will continue to be quite fruitful for this research. Accurate techniques to measure properties of larger clusters need to be developed, guided perhaps by theoretical predictions. We hope that the present work provides the stimulus for further theoretical as well as experimental approaches.

X. Acknowledgments

This article is dedicated to the memory of Professor Derek Lindsay, whose contributions to this field are considerable. We further acknowledge the efforts of our postdoctoral fellows, Zhendong Hu, Huaiming Wang, and Li Fang, who have contributed many hours of high-quality work to this research. In addition, we recognize the work of our Ph.D. students including Bo Shen, Qinwei Zhou, Jian-Guo Dong, Robert Craig, Hanae Haouri, Alberto Vivoni, Xiaole Shen, Xiaoyu Chen, Yifei Liu, Shelley Deosaran, and Haiyan Lu.

Further thanks are due to many colleagues and collaborators who have given help and advice as well as provided information on unpublished results. These include Wolfgang Harbich, Martin Moskovits, Kenneth Bosnick, Michael Pellin, Michael Morse, Doreen Leopold, Vladimir Bondybey, Giacinto Scoles, Andreas Kornath, and Marc Walters. Support for this work was generously provided by the National Science Foundation.

XI. Appendix

A. An Alternative Assignment of the Laser-Excited Fluorescence Spectrum of Copper Trimer

The earliest work on Cu_3 involved the resonance Raman spectrum in matrix isolation.[239] A progression in 354 cm^{-1} was observed and assigned to the symmetric stretch of the trimer. In a subsequent paper,[240] Moskovits reinterpreted the spectrum in terms of a dynamic Jahn−Teller molecule with a vibronic frequency of 50 cm^{-1} and a pseudorotation constant of 4.5 cm^{-1}. Observing the ESR spectrum,[241] Lindsay et al. found Cu_3 in N_2 matrices to be bent with an acute angle. This was determined by showing that only two equivalent nuclei are present.

The laser-excited gas-phase fluorescence spectrum of jet-cooled Cu_3 was obtained by Rolfing and Valentini.[151] The spectrum was assigned to a $^2E'' \rightarrow {}^2E'$ transition, and transitions from both the vibrationless band and a vibronic level at +146 cm^{-1} were obtained by exciting at two different wavelengths.

Subsequently, two independent analyses of the Cu_3 spectrum were published[153,154] in which the fluorescence spectrum was assigned on the basis of including, with the Jahn−Teller effect, a barrier to pseudorotation. Since both analyses produced essentially the same results, we arbitrarily choose the one by Truhlar, Thompson, and Mead[154](called "TTM") for comparison. Their calculations require four parameters, namely, the symmetric stretch frequency ω_a, the asymmetric stretch frequency ω_e, the linear Jahn−Teller distortion parameter k, and the quadratic Jahn−Teller barrier b. The values for these, which gave the best fit to the spectrum, were 270, 132, 1.56, and 0.274 cm^{-1}, respectively. The calculated values for the spectral frequencies and deviations from experiment are listed in the last two columns of Table A1. The standard deviation of the fit (assuming four independent parameters) is 7.5 cm^{-1}. Considering the difficulties in calculating the spectrum, this must be considered an excellent fit.

However, there are some difficulties with this analysis. First, as can be seen in the table, there are numerous lines that are observed but not fit. Second, several lines predicted by TTM to be of A symmetry (those at 16, 348, and 476 cm^{-1}) are observed in the spectrum, even though it appears that they should be of E symmetry. The symmetry of the line at 16 cm^{-1} can in fact be explained by considering a reassignment of the spectrum by Morse.[155] Morse shows that the excited-state accessed by Rolfing and Valentini is of $^2A_1'$ symmetry, while the band 146 cm^{-1} higher is of $^2E'$ symmetry. Fluorescence from the vibrationless $^2A_1'$ state can only terminate in $^2E'$ levels of the ground state, while fluorescence from the $^2E'$ level at 146 cm^{-1} can terminate in both $^2E'$

Table A1. Assignment of the Laser-Jet Fluorescence Spectrum of Cu Trimer[a]

observed (cm^{-1})	n_1	n_2	j	calculated	difference	calculated (TTM)	difference
16a	0	0	3/2	16	0	16	0
	0	0	5/2	48	†		
99	0	0	7/2	97	2	100	−1
145a	0	1	1/2	145	0		
153	0	0	9/2	161	−8	154	−1
	0	1	3/2	161	(−8)		
	0	1	5/2	193	†		
220							
230	1	0	1/2	230	0	229	1
238	0	1	7/2	242	−4		
239	0	0	11/2	242	−3	241	−2
272	1	0	5/2	278	−6	272	0
304	0	1	9/2	306	−2	307	3
324a	1	0	7/2	327	−3		
345	0	0	13/2	339	6	348	−3
353							
358						360	−2
376a	1	1	1/2	375	1		
398	1	0	9/2	391	7	392	6
407	1	1	3/2	391	16	421	−14
459	0	0	15/2	452	7		
466	2	0	1/2	460	6	474	−8
	1	0	11/2	472	(−6)		
484	0	1	13/2	484	0	476	8
520	1	2	1/2	520	0	521	−1
543	1	1	9/2	536	7		
556	2	0	7/2	557	−1	561	−5
579	0	0	17/2	581	−2	568	11
625	2	0	9/2	621	4	611	14
665a	1	3	1/2	665	0		
681	1	0	15/2	682	−1		
693	3	0	1/2	690	3		
718a	1	1	13/2	714	4		
750a	2	2	1/2	750	0		
780	3	0	7/2	787	−7		
804	1	0	17/2	811	−7		
836	3	1	1/2	835	1		
889	0	0	21/1	888	−1		

[a] The equation used is $\omega(n_1,n_2,j) = (n_1 + 1/2)\omega_a + (n_2 + 1/2)\omega_e + \alpha j^2$ (minus the zero-point energy), where $\omega_a = 230\ cm^{-1}$, $\omega_e = 145\ cm^{-1}$, and $\alpha = 8.07\ cm^{-1}$. Where there is a difference in parentheses, two assignments are possible (see the previous calculation). Where a dagger is listed (†), the predicted line is not observed.

and $^2A_1'$ levels of the ground state. In the table we have marked lines observed only from the upper level as "a", indicating that by this assignment they are likely to terminate only in states of $^2A_1'$ symmetry. Thus, the vibronic level at 16 cm^{-1} can be of $^2A'$ symmetry. The 348 and 476 cm^{-1} lines predicted by TTM, however, can still not be explained. Third, the value for ω_a (266 cm^{-1}), while much better than the value determined from the Raman spectrum (354 cm^{-1}), is still somewhat high. As discussed above, we have found the rules of Ozin and McIntosh[215] to be an excellent guide for the prediction of the force constants of higher clusters from that of the dimer, as illustrated in Tables 8 and B1. Using the measured Cu dimer force constant[149,242] of 1.33 mdyne/Å, we predict a trimer force constant of 0.67 mdyne/Å or a trimer symmetric stretch frequency ω_a of approximately 230 cm^{-1}.

It is with these considerations in mind that we attempt to fit the spectrum of Cu_3 using only three parameters and assuming only a linear Jahn−Teller effect

$$\omega(n_1, n_2, j) = (n_1 + 1/2)\omega_a + (n_2 + 1/2)\omega_e + \alpha j^2$$

where we take $\omega_a = 230\ cm^{-1}$ and $\omega_e = 145\ cm^{-1}$. We find a progression in ω_a of three lines at 230, 465, and 693 cm^{-1}, which fits quite well. For lines with $n_1 = n_2 = 0$ and $j = 1/2$ to 21/2, we use a quadratic least-squares fit to determine $\alpha = 8.07(6)\ cm^{-1}$. Using these results, various other combinations may be assigned, as shown in Table A1. The standard deviation of the fit (assuming three parameters) is 5.2 cm^{-1}, which compares favorably to that of TTM (7.5 cm^{-1}). In all, 31 out of 34 of the observed lines are assigned with this fit, compared with only 17 by TTM.

This fit has several advantages. It is conceptually simpler and requires only three independent parameters. Furthermore, many more lines are fit than that of TTM, although there are still two lines (353 and 358 cm^{-1}) which cannot be explained. (These, however, appear to be poorly resolved lines overlapping with the line at 345 cm^{-1}.) Additionally, the symmetric stretch vibrational frequency is more in line with what might be expected for a trimer, by comparison with other observed trimers. We must also consider symmetry. Lines which terminate in levels with $j = 1/2$, 5/2, 7/2, 11/2, etc., are of e′ vibronic

Table B1. Experimental Force Constants (mdyne/Å) for Various Metal Clusters M_n[a]

n	Li	Na	K	Rb	Cs	Mg	P	As
2	0.257	0.173	0.093	0.083	0.069	0.071	5.46	4.07
3			0.051(0.047)	0.049(0.042)	0.041(0.035)			
4	0.110(0.103)	0.091(0.069)	0.050(0.037)			0.15(0.024)	1.72(1.82)	1.38(1.36)

[a] The tetramers ($n = 4$) of Li, Na, and K are of rhomboidal geometry (D_{2h}), while those of Mg, P, and As are tetrahedral (T_d). Values in parentheses are force constants calculated from the dimer force constants using the scheme of Ozin and McIntosh (Ozin, G. A.; McIntosh, D. F. *J. Phys. Chem.* **1986**, *90*, 5756).

symmetry, while those with $j = 3/2, 9/2, 15/2$, etc., are of a_1 or a_2 symmetry. Once again, the line at 16 cm^{-1} is nicely explained. Most of the other lines marked "a" can fit our assignment, if we assume some vibronic mixing with excited levels of the e′ vibration, enabling observation of resultant a_1a_2 modes. Only the line at 324 cm^{-1} (assigned [1,0,7/2], strictly e′) cannot be explained with this analysis.

This assignment has, however, one additional disadvantage: it predicts two lines marked by † in the table which are not observed. Most serious is the absence of the (0,0,5/2) line predicted to be at 48 cm^{-1}, but we also expect to see the (0,1,5/2) line at 193 cm^{-1}. Both lines are predicted to be in a region of the spectrum which is relatively clear of other lines, yet there appears no trace of a line in either region. It is difficult to compare this with TTM, who do not report calculated intensities. However, Zwanziger, Whetten, and Grant[153] independently carried out the same calculation as TTM, with essentially the same parameters, and they include calculated intensities. They report numerous serious discrepancies in this regard. For example, the line at 154 cm^{-1} is predicted to have very low intensity in emission from the excited ($^2E'$) state but is observed at almost the same strength as from the origin. Conversely, the line at 304 cm^{-1} is predicted to have twice the intensity from the excited ($^2E'$) state but is observed with almost no intensity from the origin. Similar problems are obtained for lines at 462 and 581 cm^{-1}. Thus, both the present analysis and the previous ones fail to predict the correct intensities for at least several lines.

We should also point out several other difficulties with the present approach. The strong linear Jahn−Teller effect with parameters obtained ($\omega_e = 145$ cm^{-1} and $\alpha = 8.07$ cm^{-1}) correspond to the dimensionless Moffitt−Thorson parameter[243] $D = \omega_e/4\alpha$ of about 4.5, which is smaller than the usually stated limit of validity of around 5. Furthermore, the theory also fails when the total energy of those levels in which all the energy is in the e′ vibrational mode or in pseudorotation is greater than $\omega_e^2/4\alpha$ which is around 577 cm^{-1}. Thus, the assignments of the bands at 579 and 889 cm^{-1} must be regarded as suspect. Furthermore, several of the assignments represent emission to levels with quite high values of *j*, for which we might expect rather low intensities. Despite these difficulties, the fit is remarkable, considering the few adjustable parameters involved, and further work on this approach to the spectrum of Cu trimer is planned.

In summary, if we compare the results of the assignment presented here with that of TTM, this assignment fits more of the observed spectrum (31 lines compared with 17 lines out of 34) with less parameters (3 as opposed to 4). In addition, the standard deviation of the fit is better (5.2 vs 7.5). Neither approach can account for all the intensities observed nor all symmetries, and the present assignment predicts two lines, which are not observed.

B. Force Constants of Several Non-Transition-Metal Clusters

In this article we have focused on transition-metal and lanthanide clusters, but in light of recent work by Kornath[217,244,245] on the matrix isolation Raman spectroscopy of several other metal species, it is worth examining briefly how well the rules of Ozin and McIntosh[215] may be applied. In Table B1 we list the force constants for various clusters, including the dimers and the trimers of K, Rb, and Cs, the tetramers of Li, Na, and K (which are of rhomboidal D_{2h} structure) and Mg, P, and As (which are tetrahedral T_d). These force constants were calculated from the observed frequencies using a simple central force approximation but are found to agree closely with the results of density functional calculations carried out by Kornath.[246] The values in Table B1 in parentheses are force constants calculated according to the rules of Ozin and McIntosh. As discussed above, these involve calculating, for a cluster of size *n*, the sum of the number of atoms to which each atom in a bond is connected (α_n). Then the factor $\beta_n = 2/(\alpha_n)$ is multiplied by the dimer force constant, $k^{(n)} = \beta_n k^{(2)}$. For a trimer which is an equilateral triangle, this factor is $\beta_3 = 1/2$, while for a linear trimer it is 2/3. For C_{2v} symmetry, we might expect a ratio somewhere between 1/2 and 2/3. For a tetrahedral tetramer (T_d) the factor is $\beta_4 = 1/3$, while for a rhomboidal tetramer (D_{2h}) with equal bonds the factor is $\beta_4 = 2/5$.

The results for various clusters (Table B1) show a good fit for all the clusters with the exception of Mg_4, where a discrepancy of more than a factor of 6 is obtained. This is attributed to the onset of covalent bonding in the larger cluster, compared with the relatively weak van der Waals bonding expected in the dimer. This is quite similar to the comparison of Mn_2 and Mn_3 force constants discussed in section V above. The excellent results for the other clusters are just what might be expected for s- or sp-bonded metals, since simple redistribution of the bond order (electron density) on forming higher clusters is a reasonable expectation. The original rules were intended for silver clusters, which, due to the $4d^{10}5s^1$ atomic configuration, are expected to involve only s electrons in bonding. It is of considerable interest for our work here that these rules can be so successfully

extended to transition metals with bonding d electrons as well.

XII. References

(1) Sicily, E. *Thirteenth International School*; 1987. See: G. Benedek et al. *Elemental and Molecular Clusters*; Springer-Verlag: New York, 1988.
(2) Fifth International Meeting on Small Particles and Metal Clusters, Konstanz, Germany, 1990. See: *Z. Phys.* **1991**, D19. Sixth International Meeting on Small Particles and Metal Clusters, Chicago, IL, 1992. See: *Z. Phys.* **1993**, D26.
(3) International Symposium on the Physics and Chemistry of Small Clusters, NATO Advanced Workshop, Richmond, VA, 1991. See: *Physics and Chemistry of Finite Systems: From Clusters to Crystals*; Jena, P., Khanna, S. N., Rao, B. K., Eds.; Kluwer: Dordrecht, 1992.
(4) Symposium on Clusters and Cluster Assembled Materials, Materials Research Society Meeting, Boston, MA, 1990. See: MRS Symposium Series 206, 1991.
(5) *First International Conference on Nuclear and Atomic Clusters*, Turku, Finland, 1991. *Second International Conference on Nuclear and Atomic Clusters*, Santorini, Greece, 1993.
(6) Proceedings of the 10th International IUPAC Conference. *High Temp. Mater. Chem.* **2000**, 15.
(7) Weltner, W.; Van Zee, R. J. *Annu. Rev. Phys. Chem.***1984**, *35*, 291.
(8) Morse, M. D. *Chem. Rev.* **1986**, *86*, 1049.
(9) Moskovits, M. *Metal Clusters*; Wiley: New York, 1986.
(10) Duncan, M. A. *Advances in Metal and Semiconductor Clusters*; JAI Press: Greenwich, CT, 1993.
(11) Balasubramanian, K. *J. Chem. Phys.* **1989**, *91*, 307.
(12) Barden, C. J.; Rienstra-Kiracofe, J. C.; Shaefer, H. F., III *J. Chem. Phys.* **2000**, *113*, 690.
(13) Cai, M. F.; Dzgan, T. P.; Bondybey, V. E. *Chem. Phys. Lett.* **1988**, *155*, 430.
(14) Efremov, V. M.; Samoilova, A. N.; Kozhukhovsky, V. B.; Gurvich, L. V. *J. Mol. Spectrosc.* **1978**, *73*, 430.
(15) Heimbrook, L. A.; Rasanen, M.; Bondybey, V. E. *J. Phys. Chem.* **1987**, *91*, 2468.
(16) Fu, Z.; Lemire, G. W.; Hamrick, Y. M.; Taylor, S.; Shui, J. C.; Morse, M. D. *J. Chem. Phys.* **1988**, *88*, 3524.
(17) Simard, B.; Lebeault-Dorget, M. A.; Marijnissen, A.; ter Meulen, J. J. *J. Chem. Phys.* **1998**, *108*, 9668.
(18) Doverstäl, M.; Lindgren, B.; Sassenberg, U.; Arrington, C. A.; Morse, M. D. *J. Chem. Phys.* **1992**, *97*, 7087.
(19) James, A. W.; Kowalczyk, P.; Langlois, E.; Campbell, M. D.; Ogawa, A.; Simard, B. *J. Chem. Phys.* **1994**, *101*, 4485.
(20) Spain, E. M.; Behm, J. M.; Morse, M. D. *J. Chem. Phys.* **1992**, *96*, 2511.
(21) Leopold, D. G.; Lineberger, W. C. *J. Chem. Phys.* **1986**, *85*, 51.
(22) Cooper, J.; Zare, R. N. *J. Chem. Phys.* **1968**, *48*, 942.
(23) Hall, J. L.; Siegel, M. W. *J. Chem. Phys.* **1968**, *48*, 943.
(24) Rice, J. K.; Kupperman, A.; Trajmar, S. *J. Chem. Phys.* **1968**, *48*, 945.
(25) Hu, Z.; Dong, J. G.; Lombardi, J. R.; Lindsay, D. M. *J. Chem. Phys.* **1994**, *101*, 95.
(26) Hu, Z.; Shen, B.; Zhou, Q.; Deosaran, S.; Lombardi, J. R.; Lindsay, D. M.; Harbich, W. *J. Chem. Phys.* **1991**, *95*, 2206.
(27) Shen, X.; Fang, L.; Chen, X.; Lombardi, J. R. *J. Chem. Phys.* **2000**, *113*, 2233.
(28) Chen, X.; Fang, L.; Shen, X.; Lombardi, J. R. *J. Chem. Phys.* **2000**, *112*, 9780.
(29) Bondybey, V. E.; Smith, A. M.; Agreiter, J. *Chem. Rev.* **1996**, *96*, 2113.
(30) Wang, L.-S.; Li, X.; Zhang, H.-F. *Chem. Phys.* **2000**, *262*, 53.
(31) Fedrigo, S.; Harbich, W.; Buttet, J. *Phys. Rev. B* **1993**, *47*, 10706.
(32) Fedrigo, S.; Harbich, W.; Buttet, J. *J. Chem. Phys.* **1993**, *99*, 5712.
(33) DiLella, D. P.; Gohin, A.; Lipon, R. H.; McBreen, P.; Moskovits, M. *J. Chem. Phys.* **1980**, *73*, 4282.
(34) Knight, L.B., Jr.; Van Zee, R. J.; Weltner, W., Jr. *Chem. Phys. Lett.* **1983**, *94*, 296.
(35) Pápai, I.; Castro, M. *Chem. Phys. Lett.* **1997**, *267*, 551.
(36) Moskovits, M.; DiLella, D. P.; Limm, W. *J. Chem. Phys.* **1984,** *80*, 626.
(37) Gingerich, K. A. *Faraday Symp. Chem. Soc.* **1980**, *14*, 109.
(38) Verhaegen, G.; Smoes, S.; Drowart, J. *J. Chem. Phys.* **1964**, *40*, 239.
(39) Haslett, T. L.; Moskovits, M.; Weitzman, A. L. *J. Mol. Spectrosc.* **1989**, *135*, 259.
(40) Knight, L. B., Jr.; Woodward, R. W.; Van Zee, R. J.; Weltner, W., Jr. *J. Chem. Phys.* **1983**, *79*, 5820.
(41) Walch, S. P.; Bauschlicher, C. W., Jr. *J. Chem. Phys.* **1983**, *79*, 3590. Walch, S. P.; Bauschlicher, C. W., Jr. *J. Chem. Phys.* **1985**, *83*, 5735.
(42) Fang, L.; Chen, X.; Shen, X.; Liu, Y.; Lindsay, D. M.; Lombardi, J. R. *Fiz. Nizk. Temp.* **2000**, *26*, 1011. See also: *Low Temp. Phys.* **2000**, *26*, 752.
(43) Yang, D. S.; Simard, B.; Hackett, P. A.; Bréces, A.; Zgierski, M. Z. *Int. J. Mass Spectrom. Ion Processes.* **1996**, *159*, 65.
(44) Dai, D.; Balasubramanian, K. *J. Chem. Phys.* **1993**, *98*, 7098.
(45) Liu, Y.; Fang, L.; Shen, X.; Chen, X.; Lombardi, J. R.; Lindsay, D. M. *Chem. Phys.* **2000**, *262*, 25.
(46) Fang, L.; Chen, X.; Shen, X.; Lombardi, J. R. *J. Phys. Chem. A* **2000**, *104*, 9153.
(47) Fang, L.; Chen, X.; Shen, X.; Lombardi, J. R. *J. Chem. Phys.* **2000**, *113*, 10202.
(48) Doverstål, M.; Karlsson, L.; Lindgren, B.; Sassenberg, U. *Chem. Phys. Lett.* **1997**, *270*, 273. See also ref 18.
(49) Cooper, W. F.; Clarke, G. A.; Hare, C. A. *J. Phys. Chem.* **1972**, *76*, 2268.
(50) Cossé, C.; Fouassier, M.; Mejean, T.; Tranquille, M.; DiLella, D. P.; Moskovits, M. *J. Chem. Phys.* **1980**, *73*, 6076.
(51) Kant, A.; Lin, S. S. *J. Chem. Phys.* **1969**, *51*, 1644.
(52) Doverstål, M.; Karlsson, L.; Lindgren, B.; Sassenberg, U. *J. Phys. B: At., Mol. Opt. Phys.* **1998**, *31*, 795.
(53) Hu, Z.; Zhou, Q.; Lombardi, J. R.; Lindsay, D. M. In *Physics and Chemistry of Finite Systems: From Clusters to Crystals*; Jena, P., Khanna, S. N., Rao, B. K., Eds.; Kluwer: The Netherlands, 1992; p 969.
(54) Arrington, C. A.; Blume, T.; Morse, M. D.; Doverstål, M.; Sassenberg, U. *J. Phys. Chem.* **1994**, *98*, 1398.
(55) Haouari, H.; Wang, H.; Craig, R.; Lombardi, J. R.; Lindsay, D. M. *J. Chem. Phys.* **1995**, *103*, 9527.
(56) Dai, D.; Balasubramanian, K. *Chem. Phys. Lett.* **1994**, *231*, 352.
(57) Hu, Z.; Dong, J. G.; Lombardi, J. R.; Lindsay, D. M. *J. Phys. Chem.* **1993**, *97*, 9263.
(58) Wang, H.; Hu, Z.; Haouari, H.; Craig, R.; Liu, Y.; Lombardi, J. R.; Lindsay, D. M. *J. Chem. Phys.* **1997**, *106*, 8339.
(59) Dai, D.; Roszak, S.; Balasubramanian, K. *Chem. Phys. Lett.* **1999**, *308*, 495.
(60) Langridge-Smith, P. R. R.; Morse, M. D.; Hansen, G. P.; Smalley, R. E.; Merer, A. J. *J. Chem. Phys.* **1984**, *80*, 593.
(61) Calaminici, P.; Köster, A. M.; Carrington, T., Jr.; Roy, P. N.; Russo, N.; Salahub, D. R. *J. Chem. Phys.* **2001**, *114*, 4036.
(62) Spain, E. M.; Morse, M. D. *J. Phys. Chem.* **1992**, *96*, 2479.
(63) Yang, D. S.; James, A. M.; Rayner, D. M.; Hackett, P. A. *Chem. Phys. Lett.* **1994**, *231*, 177.
(64) Moskovits, M.; Limm, W. *Ultramicroscopy* **1986**, *20*, 83.
(65) Hu, Z.; Shen, B.; Zhou, Q.; Deosaran, S.; Lombardi, J. R.; Lindsay, D. M. *SPIE* **1991**, *1599*, 65.
(66) James, A. M.; Kowalczyk, P.; Fournier, R.; Simard, B. *J. Chem. Phys.* **1993**, *99*, 8504.
(67) James, A. M.; Kowalczyk, P.; Langlois, E.; Campbell, M. D.; Ogawa, A.; Simard, B. *J. Chem. Phys.* **1994**, *101*, 4485.
(68) Wang, H.; Craig, R.; Haouari, H.; Liu, Y.; Lombardi, J. R.; Lindsay, D. M. *J. Chem. Phys.* **1996**, *105*, 5355.
(69) Leopold, D. G. Private communication.
(70) Heaven, M. W.; Stewart, G. M.; Buntine, M. A.; Metha, G. F. *J. Phys. Chem. A* **2000**, *104*, 3308.
(71) Hu, Z.; Shen, B.; Lombardi, J. R.; Lindsay, D. M. *J. Chem. Phys.* **1992**, *96*, 8757.
(72) Fang, L.; Shen, X.; Chen, X.; Lombardi, J. R. *Chem. Phys. Lett.* **2000**, *332*, 299.
(73) Wang, H.; Craig, R.; Haouari, H.; Dong, J. G.; Hu, J.; Vivoni, A.; Lombardi, J. R.; Lindsay, D. M. *J. Chem. Phys.* **1995**, *103*, 3289.
(74) Herzberg, G. *Infrared and Raman Spectra*; D. Van Nostrand Co.: Princeton, 1966.
(75) Bondybey, V. E.; English, J. H. *Chem. Phys. Lett.* **1983**, *94*, 443.
(76) Casey, S. M.; Leopold, D. G. *J. Phys. Chem.* **1993**, *97*, 816.
(77) Hilpert, K.; Ruthardt, K. *Ber. Bunsen-Ges. Phys. Chem.* **1987**, *91*, 724.
(78) Simard, B.; Lebeault-Dorget, M.-A.; Marijnissen, A.; ter Meulen, J. J. *J. Chem. Phys.* **1998**, *108*, 9668.
(79) DiLella, D. P.; Limm, W.; Lipson, R. H.; Moskovits, M.; Taylor, K. V. *J. Chem. Phys.* **1982**, *77*, 5263.
(80) Moskovits, M.; Limm, W.; Mejean, T. *J. Phys. Chem.* **1985**, *89*, 3886.
(81) Moskovits, M.; Limm, W.; Mejean, T. *J. Chem. Phys.* **1985**, *82*, 4875.
(82) Fang, L.; Davis, B.; Lu, H.; Lombardi, J. R. *J. Phys. Chem. A* **2001**, *105*, 9375.
(83) Pellin, M. J.; Foosnaes, T.; Gruen, D. M. *J. Chem. Phys.* **1981**, *74*, 5547.
(84) Simard, B.; Lebeault-Dorget, M.; Marijnissen, A.; ter Meulen, J. J. *J. Chem. Phys.* **1998**, *108*, 9668.
(85) Fang, L.; Davis, B.; Lu, H.; Chen, X.; Shen, X.; Lombardi, J. R. *Chem. Phys. Lett.* **2002**, *352*, 70.
(86) Kraus, D.; Lorenz, M.; Bondybey, V. E. *Phys. Chem. Commun.* **2001**, 10.
(87) Hu, Z.; Dong, J. G.; Lombardi, J. R.; Lindsay, D. M. *J. Chem. Phys.* **1992**, *97*, 8811.
(88) Nesbet, R. K. *Phys. Rev. A* **1964**, *135*, 460.

(89) Baumann, C. A.; Van Zee, R. J.; Bhat, S. V.; Weltner, W., Jr. *J. Chem. Phys.* **1983**, *78*, 190.
(90) Kant, A.; Lin, S.; Strauss, B. *J. Chem. Phys.* **1968**, *49*, 1983.
(91) Bier, K. D.; Haslett, T. L.; Kirkwood, A. D.; Moskovits, M. *J. Chem. Phys.* **1988**, *89*, 6.
(92) Brewer, L.; Winn, J. S. *Faraday Symp. Chem. Soc.* **1980,** *14*, 126.
(93) Miedema, A. R.; Gingerich, K. A. *J. Phys. B* **1979**, *12*, 2081.
(94) Cotton, F. A.; Shive, L. *Inorg. Chem.* **1975,** *14***,** 2032.
(95) Leopold, D. G.; Miller, T. M.; Lineberger, W. C. *J. Am. Chem. Soc.* **1986**, *108*, 178.
(96) Harris, J.; Jones, R. O. *J. Chem. Phys.* **1979**, *70*, 830.
(97) Purdum, H.; Montano, P. A.; Shenoy, G. K.; Morrison, T. *Phys. Rev. B* **1982**, *25*, 4412.
(98) Moskovits, M.; DiLella, D. P. *J. Chem. Phys.* **1980**, *73*, 4917.
(99) Leopold, D. G.; Almlof, J.; Lineberger, W. C.; Taylor, P. R. *J. Chem. Phys.* **1988**, *88*, 3780.
(100) Lin, S.; Kant, A. *J. Phys. Chem.* **1969**, *73*, 2450.
(101) Haslett, T. L.; Moskovits, M.; Weitzman, A. L. *J. Mol. Spectrosc.* **1989**, *135*, 259.
(102) Lian, L.; Su, C. X.; Armentrout, P. B. *J. Chem. Phys.* **1992**, *97*, 4072.
(103) Leopold, D. G.; Almlof, J.; Lineberger, W. C.; Taylor, P. R. *J. Chem. Phys.* **1988**, *88*, 3780.
(104) Nour, E. M.; Alfaro-Franco, C.; Gingerich, K. A.; Laane, J. *J. Chem. Phys.* **1987**, *86*, 4779.
(105) Haslett, T. L.; Bosnick, K. A.; Fedrigo, S.; Moskovits, M. *J. Chem. Phys.* **1999**, *111*, 6456.
(106) Gutsev, G. L.; Khanna, S. N.; Jena, P. *Phys. Rev. B* **2000**, *62*, 1604.
(107) Castro, M.; Jamorski, C.; Salahub, D. R. *Chem. Phys. Lett.* **1997**, *271*, 133.
(108) Das, K. K.; Balasubramanian, K. *J. Chem. Phys.* **1991**, *95*, 2568.
(109) Cotton, F. A.;Shim, I. *J. Am. Chem. Soc.* **1982**, *104*, 7025.
(110) Wang, H.; Liu, Y.; Haouari, H.; Craig, R.; Lombardi, J. R.; Lindsay, D. M.*J. Chem. Phys.* **1997**, *106*, 6534.
(111) Miedema, A. R.; Gingerich, K. A. *J. Phys. B: At., Mol. Phys.* **1979**, *12*, 2081.
(112) Cotton, F. A.; Walton, R. A. *Multiple Bonds Between Metal Atoms*; Wiley: New York, 1982.
(113) Jamorski, C.; Martinez, A.; Castro, M.; Salahub, D. R. *Phys. Rev. B* **1997**, *55*, 10905.
(114) Castro, M.; Jamorski, C.; Salahub, D. R. *Chem. Phys. Lett.* **1997**, *271*, 133.
(115) Dong, J. G.; Hu, Z. H.; Craig, R.; Lombardi, J. R.; Lindsay, D. M. *J. Chem. Phys.* **1994**, *101*, 9280.
(116) Kant, A.; Strauss, B. *J. Chem. Phys.* **1964**, *41*, 3806.
(117) Hales, D. A.; Su, C. X.; Lian, L.; Armentrout, P. B. *J. Chem. Phys.* **1994**, *100*, 1049.
(118) Van Zee, R. J.; Hamrick, Y. M.; Li, S.; Weltner, W., Jr. *Chem. Phys. Lett.* **1992**, *195*, 214.
(119) Balasubramanian, K.; Liao, D. W. *J. Phys. Chem.* **1989**, *93*, 3989.
(120) Wang, H.; Haouari, H.; Craig, R.; Liu, Y.; Lombardi, J. R.; Lindsay, D. M. *J. Chem. Phys.* **1997**, *106*, 2101.
(121) Cocke, D. L.; Gingerich, G. A. *J. Chem. Phys.* **1974**, *60*, 1958.
(122) Langenberg, J. D.; Morse, M. D. *J. Chem. Phys.* **1998**, *108*, 2331.
(123) Fang, L.; Shen, X.; Chen, X.; Lombardi, J. R. *J. Chem. Phys.* **2000**, *113*, 7178.
(124) Ozin, G. A.; Lee Hanlan, A. J. *Inorg. Chem.* **1979**, *18*, 1781.
(125) Morse, M. D.; Hansen, G. P.; Langridge-Smith, P. R. R.; Zheng, L. S.; Geusic, M. E.; Michalopoulos, D. L.; Smalley, R. E. *J. Chem. Phys.* **1984**, *80*, 5400.
(126) Pinegar, J. C.; Langenberg, J. D.; Arrington, C. A.; Spain, E. M.; Morse, M. D. *J. Chem. Phys.* **1995**, *102*, 666.
(127) Wang, H.; Haouari, H.; Craig, R.; Lombardi, J. R.; Lindsay, D. M. *J. Chem. Phys.* **1996**, *104*, 3420.
(128) Moskovits, M.; DiLella, D. P. *J. Chem. Phys.* **1980**, *72*, 2267.
(129) Ho, J.; Polak, M. L.; Ervin, K. M.; Lineberger, W. C. *J. Chem. Phys.* **1993**, *99*, 8542.
(130) Ho, J.; Ervin, K. M.; Polak, M. L.; Giles, M. K.; Lineberger, W. C. *J. Chem. Phys.* **1991**, *95*, 4845
(131) Shim, I.; Gingerich, K. A. *J. Chem. Phys.* **1984**, *80*, 5107.
(132) Lin, S.S.; Strauss, B.; Kant, A. *J. Chem. Phys.* **1969**, *51*, 2282.
(133) Ervin, K. M.; Ho, J.; Lineberger, W. C. *J. Chem. Phys.* **1988**, *89*, 4514.
(134) Ho, J.; Polak, M. L.; Ervin, K. M.; Lineberger, W. C. *J. Chem. Phys.* **1993**, *99*, 8542.
(135) Fabbi, J. C.; Langenberg, J. D.; Costello, Q. D.; Morse, M. D.; Karlsson, L. *J. Chem. Phys.* **2001**, *115*, 7543.
(136) Wang, H.; Liu, Y.; Haouari, H.; Craig, R.; Lombardi, J. R.; Lindsay, D. M. *J. Phys. Chem.* **1997**, *101*, 7036.
(137) Taylor, S.; Lemire, G. W.; Hamrick, Y. M.; Fu, Z.; Morse, M. D. *J. Chem. Phys.* **1988**, *89*, 5517.
(138) Cui, Q.; Musaev, D. G.; Morokuma, K. *J. Chem. Phys.* **1998**, *108*, 8418.
(139) Balasubramanian, K. *J. Chem. Phys.* **1987**, *87*, 6573.
(140) Airola, M. B.; Morse, M. D. *J. Chem. Phys.* **2002,** *116*, 1313.
(141) Ervin, K. M.; Ho, J.; Lineberger, W. C. *J. Chem. Phys.* **1998**, *89*, 4514.
(142) Kua, J.; Goddard, W. A., III *J. Phys. Chem. B* **1998**, *102*, 9481.
(143) Bondybey, V. E. *J. Chem. Phys.* **1982**, *77*, 3771.
(144) Gole, J. L.; English, J. H.; Bondybey, V. E. *J. Phys. Chem.* **1982**, *86*, 2560.
(145) Moskovits, M.; Hulse, J. E. *J. Chem. Phys.* **1977**, *67*, 4271.
(146) O'Keefe, A.; Scherer, J. J.; Cooksey, A. L.; Sheeks, R.; Heath, J.; Saykally, R. J. *Chem. Phys. Lett.* **1990**, *172*, 214.
(147) Page, R. H.; Gudeman, C. S. *J. Chem. Phys.* **1991**, *94*, 39.
(148) Powers, D. E.; Hansen, S. G.; Geusic, M. E.; Michalopoulos, D. L.; Smalley, R. E. *J. Chem. Phys.* **1983**, *78*, 2866.
(149) Ram, R. S.; Jarman, C. N.; Bernath, P. F. *J. Mol. Spectrosc.* **1992**, *156*, 468.
(150) Morse, M. D. *Advances In Metal and Semiconductor Clusters*; JAI Press: Greenwich, CT, 1993; Vol. I (Spectroscopy and Dynamics), p 83.
(151) Morse, M. D.; Hopkins, J. B.; Langridge-Smith, P. R. R.; Smalley, R. E. *J. Chem. Phys.* **1983**, *79*, 5316.
(152) Rohlfing, E. A.; Valentini, J. J. *Chem. Phys. Lett.* **1986**, *126*, 113.
(153) Zwanziger, J.W.; Whetten, R. L.; Grant, E. R. *J. Phys. Chem.* **1986**, *90*, 3298.
(154) Truhlar, D.G.; Thompson, T. C.; Mead, C. A. *Chem. Phys. Lett.* **1986**, *127*, 287.
(155) Morse, M. D. *Chem. Phys. Lett.* **1987**, *133*, 8.
(156) Moskovits, M.; Hulse, J. E. *J. Phys. Chem.* **1977**, *81*, 2004.
(157) Moskovits, M. *Chem. Phys. Lett.* **1985**, *118*, 111.
(158) DiLella, D. P.; Taylor, K. V.; Moskovits, M. *J. Phys. Chem.* **1983**, *87*, 524.
(159) Lindsay, D. M.; Thompson, G. A.; Wang, Y. *J. Phys. Chem.* **1987**, *91*, 2630.
(160) Howard, J. A.; Preston, K. F.; Sutcliffe, R. *J. Phys. Chem.* **1983**, *87*, 536.
(161) Bosnick, K. A. Dissertation, University of Toronto, 2000.
(162) Srdanov, V. I.; Pešić, D. S. *J. Mol. Spectrosc.* **1981**, *90*, 27.
(163) Brown, C. M.; Ginter, M. L. *J. Mol. Spectrosc.* **1978**, *69***,** 25.
(164) Simard, B.; Hackett, P. A.; James, A. M.; Langridge-Smith, P. R. R. *Chem. Phys. Lett.* **1991**, *186*, 415.
(165) Kremer, H. G.; Beutel, V.; Weyers, K.; Demtroder, W. *Chem. Phys. Lett.* **1992**, *193*, 331.
(166) Haslett, T. L.; Bosnick, K. A.; Fedrigo, S.; Moskovits, M. *J. Chem. Phys.* **1999**, *111*, 6456.
(167) Schulze, W.; Becker, H. U.; Minkwitz, R.; Manzel, K. *Chem. Phys. Lett.* **1978**, *55*, 59.
(168) Okazaki, T.; Saito, Y.; Kasuya, A.; Nishina, Y. *J. Chem. Phys.* **1996**, *104*, 812.
(169) Cheng, P. Y.; Duncan, M. A. *Chem. Phys. Lett.* **1988**, *152*, 341.
(170) Wedum, E. E.; Grant, E. R.; Cheng, P. Y.; Willey, K. F.; Duncan, M. A. *J. Chem. Phys.* **1994**, *100*, 6312.
(171) Wallimann, F.; Frey, H.; Leutwyler, S.; Riley, M. *Z. Phys. D* **1997**, *40*, 30.
(172) Ellis, A. M.; Robles, E. S. J.; Miller, T. A. *Chem. Phys. Lett.* **1993**, *201*, 132.
(173) Félix, C.; Sieber, C.; Harbich, W.; Buttet, J.; Rabin, I.; Schulze, W.; Ertl, G. *Chem. Phys. Lett.* **1999**, *313*, 105.
(174) Félix, C.; Sieber, C.; Harbich, W.; Buttet, J.; Rabin, I.; Schulze, W.; Ertl, G. *Phys. Rev. Lett.* **2001**, *86*, 2992.
(175) Haslett, T. L.; Bosnick, K. A.; Moskovits, M. *J. Chem. Phys.* **1998**, *108*, 3453.
(176) Bosnick, K. A.; Haslett, T. L.; Fedrigo, S.; Moskovits, M. *J. Chem. Phys.* **1999,** *111*, 8867.
(177) Harbich, W.; Fedrigo, S.; Buttet, H. *Z. Phys.* **1993**, *D26*, 138.
(178) Harbich, W.; Fedrigo, S.; Meyer, F.; Lindsay, D. M.; Lignieres, J.; Rivoal, J. C.; Kreisle, D. *J. Chem. Phys.* **1990**, *93*, 8535.
(179) Ruamps, J. *Ann. Phys. (Paris)* **1959**, *4*, 1111.
(180) Simard, B.; Hackett, P. A. *J. Mol. Spectrosc.* **1990**, *142*, 310.
(181) Bishea, G. A.; Morse, M. D. *J. Chem. Phys.* **1991**, *95*, 5646.
(182) Balasubramanian, K.; Liao, M. Z. *J. Chem. Phys.* **1987**, *86*, 5587. Balasubramanian, K.; Liao, M. Z. *Chem. Phys.* **1988**, *127*, 313.
(183) Bishea, G. A.; Morse, M. D. *J. Chem. Phys.* **1991**, *95*, 8779.
(184) Czajkowski, M. A.; Koperski, J. *Spectrochim. Acta* **1999**, *A55*, 2221.
(185) van Zee, R. D.; Blankespoor, S. C.; Zwier, T. S. *J. Chem. Phys.* **1988**, *88*, 4650.
(186) Hilpert, K. *J. Chem. Phys.* **1982**, *77*, 1425.
(187) Koperski, J.; Atkinson, J. B.; Krause, L. *Chem. Phys. Lett.* **1994**, *219*, 161.
(188) Yu, M.; Dolg, M. *Chem. Phys. Lett.* **1997**, *273*, 329.
(189) Pitzer, K. S. *Acc. Chem. Res.* **1979**, *12*, 271.
(190) Pyykko, P.; Desclaux, J. P. *Acc. Chem. Res.* **1979**, *12*, 276.
(191) Desclaux, J. P. *At. Data Nucl. Data Tables* **1973**, *12*, 311.
(192) Bishea, G. A.; Morse, M. D. *J. Chem. Phys.* **1991**, *95*, 8779.
(193) Schwerdtfeger, P.; Dolg, M. *Phys. Rev. A* **1991**, *43*, 1644.
(194) Pauling, L. *The Nature of the Chemical Bond*; Cornell University Press: Ithaca, 1960.
(195) Johnston, H. S. *Gas-Phase Reaction Rate Theory*; The Ronald Press: New York, 1966.
(196) Miedema, A. R.; Gingerich, K. A. *J. Phys. B: At., Mol. Phys.* **1979**, *12*, 2081.
(197) Badger, R. M. *J. Chem. Phys.* **1934**, *2*, 128. Badger, R. M. *J. Chem. Phys.* **1935**, *3*, 710.

(198) Herschbach, D. R.; Laurie, V. W. *J. Chem. Phys.* **1961**, *35*, 458.
(199) Weisshaar, J. C. *J. Chem. Phys.* **1989**, *90*, 1429.
(200) Cioslowski, J.; Liu, G.; Mosquera Castro, R. A. *Chem. Phys. Lett.* **2000**, *331*, 497.
(201) Guggenheimer, K. M. *Proc. Phys. Soc.* **1946**, *58*, 456.
(202) Pettifor, D. G. *Bonding and Structures of Molecules and Solids;* Clarendon Press: Oxford, 1995.
(203) Kant, A.; Lin, S. S. *Monatsh. Chem.* **1972**, *103*, 757.
(204) Dolg, M.; Stoll, H.; Preuss, H. *J. Mol. Struct. (THEOCHEM).* **1992**, *277*, 239.
(205) Schwerdtfeger, P.; Dolg, M. *Phys. Rev. A* **1991**, *43*, 1644.
(206) Van Zee, R. J.; Li, S.; Weltner, W., Jr. *J. Chem. Phys.* **1994**, *100*, 4010.
(207) Dolg, M.; Liu, W.; Kalvoda, S. *Int. J. Quantum Chem.* **2000**, *76*, 359.
(208) Klotzbücher, W. E.; Petrukhina, M. A.; Sergeev, G. B. *Mendeleev Commum.* **1994**, 5.
(209) Klotzbücher, W. E. Private communication.
(210) Klotzbücher, W. E.; Petrukhina, M. A.; Sergeev, G. B. *J. Phys. Chem. A* **1997**, *101*, 4548.
(211) Suzer, S.; Andrews, L. *J. Chem. Phys.* **1988**, *89*, 5514.
(212) Martin, W. C.; Zablubas, R.; Hagan, L. *Atomic Energy Levels-The Rare Earth Elements*; National Bureau of Standards Reference Data Series 60; U.S. Department of Commerce: Washington, D.C., 1978.
(213) This means proportional to $A\Lambda\Sigma$, where A is the molecular spin−orbit coupling constant and Λ and Σ are the projections of the orbital and spin angular momentum on the internuclear axis. For a $^3\Pi$ state, $\Lambda = 1$ and $\Sigma = -1, 0, 1$. Note that $\Omega = \Lambda + \Sigma$.
(214) Jensen, W. B. *J. Chem. Educ.* **1982**, *59*, 634.
(215) Ozin, G. A.; McIntosh, D. F. *J. Phys. Chem.* **1986**, *90*, 5756.
(216) McAdon, M. H.; Goddard, W. A., III *Phys. Rev. Lett.* **1985**, *55*, 2563.
(217) Kornath, A. Strukturaufklarung kleiner ligandenfreier Metallcluster, Thesis, Universitat Dortmund, Mai 2000.
(218) Gohel, V. B.; Acharya, C. K.; Jani, A. R. *J. Phys. F. Met. Phys.* **1985**, *15*, 279.
(219) Taylor, K. J.; Jin, C.; Conceicao, J.; Wang, L. S.; Cheshnovsky, O.; Johnson, B. R.; Nordlander, P. J.; Smalley, R. E. *J. Chem. Phys.* **1990**, *93*, 7515.
(220) Marcy, T. P.; Leopold, D. G. *Int. J. Mass Spectrom.* **2000**, *195/196*, 653.
(221) Cheng, H. S.; Wang, L.-S. *Phys. Rev. Lett.* **1996**, *77*, 51.
(222) Wu, S. R.; Desai, L. S.; Wang, L.-S. *Phys. Rev. Lett.* **1996**, *76*, 212.
(223) Wu, S. R.; Desai, L. S.; Wang, L.-S. *Phys. Rev. Lett.* **1996**, *77*, 2436.
(224) Klotzbücher, W. E.; Petrukhina, M. A.; Nemukhin, A. V.; Ermilov, A. Y.; Grigorenko, B. L. *Spectrochim. Acta* **2001**, *A57*, 1093.
(225) Koretsky, G. M.; Knickelbein, M. B. *Eur. Phys. J. D* **1998**, *2*, 273.
(226) Bonnelle, C.; Vergand, F. *J. Phys. Chem. Solids*, **1975**, *36*, 575.
(227) Douglass, D. C.; Bucher, J. P.; Bloomfield, L. A. *Phys. Rev. Lett.* **1992**, *68*, 1774.
(228) Douglass, D. C.; Cox, A. J.; Bucher, J. P.; Bloomfield, L. A. *Phys. Rev. B* **1993**, *47*, 12874.
(229) Bucher, J. P.; Bloomfield, L. A. *Int. J. Mod. Phys. B* **1993**, *7*, 1079.
(230) Song, Y.; Yang, R.; Li, D.; Wu, W. T.; Guo, Z. X. *Phys. Rev. B* **1999**, *59*, 14220.
(231) Kittel, C. *Introduction to Solid State Physics*; Wiley: New York, 1976.
(232) Xie, Y.; Blackman, J. A. *Phys. Rev. B* **2001**, *63*, 125105.
(233) Zhang, G. W.; Feng, Y. P.; Ong, C. K. *Phys. Rev. B* **1996**, *54*, 17208.
(234) Pettifor, D. G. *J. Phys. F.: Met. Phys.* **1977**, *7*, 613.
(235) Pettifor, D. G. *Solid State Phys.* **1987**, *40*, 43.
(236) Emsley, J. *The Elements*; Clarendon Press: Oxford, 1998.
(237) Yanagisawa, S.; Tsuneda, T.; Hirao, K. *J. Comput. Chem.* **2001**, *22*, 1995.
(238) Tsuchiya, T.; Abe, M.; Nakajima, T.; Hirao, K. *J. Chem. Phys.* **2001**, *115*, 4463.
(239) DiLella, D. P.; Taylor, K. V.; Moskovits, M. *J. Phys. Chem.* **1983**, *87*, 524.
(240) Moskovits, M. *Chem. Phys. Lett.* **1985**, *118*, 111.
(241) Lindsay, D. M.; Thompson, G. A.; Wang, Y. *J. Phys. Chem.* **1987**, *91*, 2630.
(242) Rolfing, E. A.; Valentini, J. J. *J. Chem. Phys.* **1986**, *84*, 6560.
(243) Longuet-Higgins, H. C. *Advances in Spectroscopy*; Thompson, H. W., Ed.; Interscience Publishers: New York, 1961; Vol. 2, p 429.
(244) Kornath, A.; Zoermer, A.; Ludwig, R. *Inorg. Chem.* **1999**, *38*, 4696.
(245) Kornath, A.; Ludwig, R.; Zoermer, A. *Angew. Chem., Int. Ed. Engl.* **1998**, *37*, 1575.
(246) Kornath, A. Private communication.

CR010425J